AD NUMBER

AD866172

LIMITATION CHANGES

TO:

Approved for public release; distribution is unlimited.

FROM:

Distribution authorized to U.S. Gov't. agencies and their contractors; Critical Technology; MAR 1970. Other requests shall be referred to Air Force Technical Application Center, VELA Seismological Cetner, Washington, DC 20333. This document contains export-controlled technical data.

AUTHORITY

usaf ltr, 25 jan 1972

ARPA Program Code No. 9F10

Acknowledgment: This research was supported by the Advanced Research Projects Agency, Nuclear Monitoring Research Office, under Project VELA-UNIFORM, and accomplished under the technical direction of the Air Force Technical Applications Center under Contract No. F33657-70-C-0100.

SEISMIC ARRAY PROCESSING TECHNIQUES

Quarterly Report No. 2

15 November 1969 through 15 February 1970

Frank H. Binder, Program Manager
Area Code 214, 358-5181, Ext 6521

TEXAS INSTRUMENTS INCORPORATED
Science Services Division
P.O. Box 5621
Dallas, Texas 75222

Contract No. F 33657-70-C-0100
Amount of Contract: $339,052
Beginning 15 July 1969
Ending 14 July 1970

Prepared for

AIR FORCE TECHNICAL APPLICATIONS CENTER
Washington, D. C. 20333

Sponsored by

ADVANCED RESEARCH PROJECTS AGENCY
Nuclear Test Detection Office
ARPA Order No. 624
AFTAC Project No. VELA/T/0701/B/ASD

3 March 1970

AFTAC Project No. VELA/T/0701/B/ASD

SEISMIC ARRAY PROCESSING TECHNIQUES

Quarterly Report No. 2

15 November 1969 through 15 February 1970

Frank H. Binder, Program Manager
Area Code 214, 358-5181, Ext 6521

TEXAS INSTRUMENTS INCORPORATED
Science Services Division
P.O. Box 5621
Dallas, Texas 75222

Contract No. F33657-70-C-0100
Amount of Contract: $339,052
Beginning 15 July 1969
Ending 14 July 1970

Prepared for

AIR FORCE TECHNICAL APPLICATIONS CENTER
Washington, D. C. 20333

Sponsored by

ADVANCED RESEARCH PROJECTS AGENCY
Nuclear Test Detection Office
ARPA Order No. 624
ARPA Program Code No. 9F10

3 March 1970

Acknowledgment: This research was supported by the Advanced Research Projects Agency, Nuclear Monitoring Research Office, under Project VELA-UNIFORM, and accomplished under the technical direction of the Air Force Technical Applications Center under Contract No. F33657-70-C-0100.

This document is subject to special export controls and each transmittal to foreign governments or foreign nationals may be made only with prior approval of Chief, AFTAC

Qualified users may request copies of this document from:

Defense Documentation Center
Cameron Station
Alexandria, Virginia 22314

TEXAS INSTRUMENTS
INCORPORATED
SCIENCE SERVICES DIVISION

3 March 1970

Headquarters
United States Air Force
AFTAC/VSC
Washington, D. C. 20333

Attention: Lt. John Woods

Subject: Second Quarterly Report Covering Period
15 November 1969 through 15 February 1970

Identification: AFTAC Project No.: VELA T/0701/B/ASD
Project Title: Seismic Array Processing Techniques
ARPA Order No.: 624
ARPA Program Code No.: 9F10
Name of Contractor: Texas Instruments Incorporated
Contract Number: F33657-70-C-0100
Effective Date of Contract: 15 July 1969
Amount of Contract: $339,052
Contract Expiration Date: 14 July 1970
Project Manager: Frank H. Binder
Area Code 214, 358-5181, Ext. 6521

SECTION I: INTRODUCTION

The research being done is divided into six broad categories:

- Adaptive techniques for designing fixed filters off-line
- On-line adaptive processing techniques
- Long-period array data analysis
- Short-period 37-element array data analysis
- Hi Resolution wavenumber spectra displays of seismic array data
- Special problems

Sections II through VII summarizes the results obtained and the work progress under each of these categories during the past quarter.

SECTION II: ADAPTIVE MCF TASK

The objective of the adaptive multichannel filter design task is to investigate adaptive filtering techniques through which a set of multichannel filters (MCFs) can be developed which will operate effectively in a fixed mode. Adaptive techniques implemented in both the time- and frequency-domain are to be studied and compared to conventional methods of designing optimum fixed MCFs in each domain.

A. TIME-DOMAIN DESIGN

Data from three different arrays for which fixed filters were developed through conventional techniques were selected for the adaptive MCF design study. Each of the arrays possessed an ambient noise field with some unique characteristics which might be encountered at other arrays.

Site 1

The first array selected is considered a relatively quiet site. The noise field is composed predominantly of low-frequency energy (below 1.0 Hz) with occasional occurrences of coherent energy with frequency of 2.0 Hz or higher. An MCF was designed in the frequency domain by the conventional Wiener process from 12 selected noise samples, each approximately 4-min long. The time-domain operators for the MCF were obtained and applied to one of the ensemble noise samples (1010). This noise sample plus two other samples were then selected for the initial adaptive design of an MCF. The noise samples were divided into 25-sec segments. A segment from each noise sample was adaptively processed using the basic maximum-likelihood adaptive algorithm, starting with a convergence rate approximately equal to 0.25 of maximum and letting the rate exponentially decay. A second segment from each of the three noise samples was then processed in reverse order of the preceding segments.

At the end of the adaptive processing the filter was then applied in a fixed mode to noise sample 1010. The output spectrum of the adaptively-designed MCF was compared to the spectra of a Wiener MCF and a straight-

summation process (Figure 1). Comparison indicates that the MCF adapted very well for the low-frequency energy, but the rejection level of the Wiener MCF on the higher-frequency energy was not reached. However, as stated earlier, the high-frequency energy does not occur very frequently and is only present in one (NS 1010) of the three noise samples processed for the adaptive design.

How rapidly the low-frequency energy is adapted to by the adaptive output trace when processing at a convergence rate of 0.25 of maximum is shown in Figure 2. The adaptive output during the first 50 seconds of adaption, starting with a straight-summation process, is compared to the output of the straight summation during that same time. A single input channel is included for reference.

Site 2

The second site used in this study has an extremely high ambient noise field. A non-time stationary low-frequency component (0.5 to 1.0 Hz) exists in approximately half of the 15 noise samples chosen for the conventional Wiener MCF design. However, the dominating energy is the spacially-coherent surface-mode energy existing in the 1.4-Hz to 3.0-Hz frequency band. This energy appears to be rather time-stationary except for one area (2.1 Hz). The array response provides very good rejection of this energy and Wiener processing of the noise provides additional noise rejection.

Two representative noise samples were adaptively processed at a convergence rate of 0.25 of maximum. Power spectra were computed from the adaptive output for each noise sample and are compared in Figure 3 to the spectra for the Wiener MCF and the summation process. The most significant improvement by adaptive processing over the Wiener MCF occurs in the area of 1.46 Hz, where the adaptive process is able to level the spectra out. Mean-square improvements in the 1-Hz to 3-Hz frequency band by adaptive processing over the Wiener MCF of 0.4 and 2.5 db were obtained on the two noise samples.

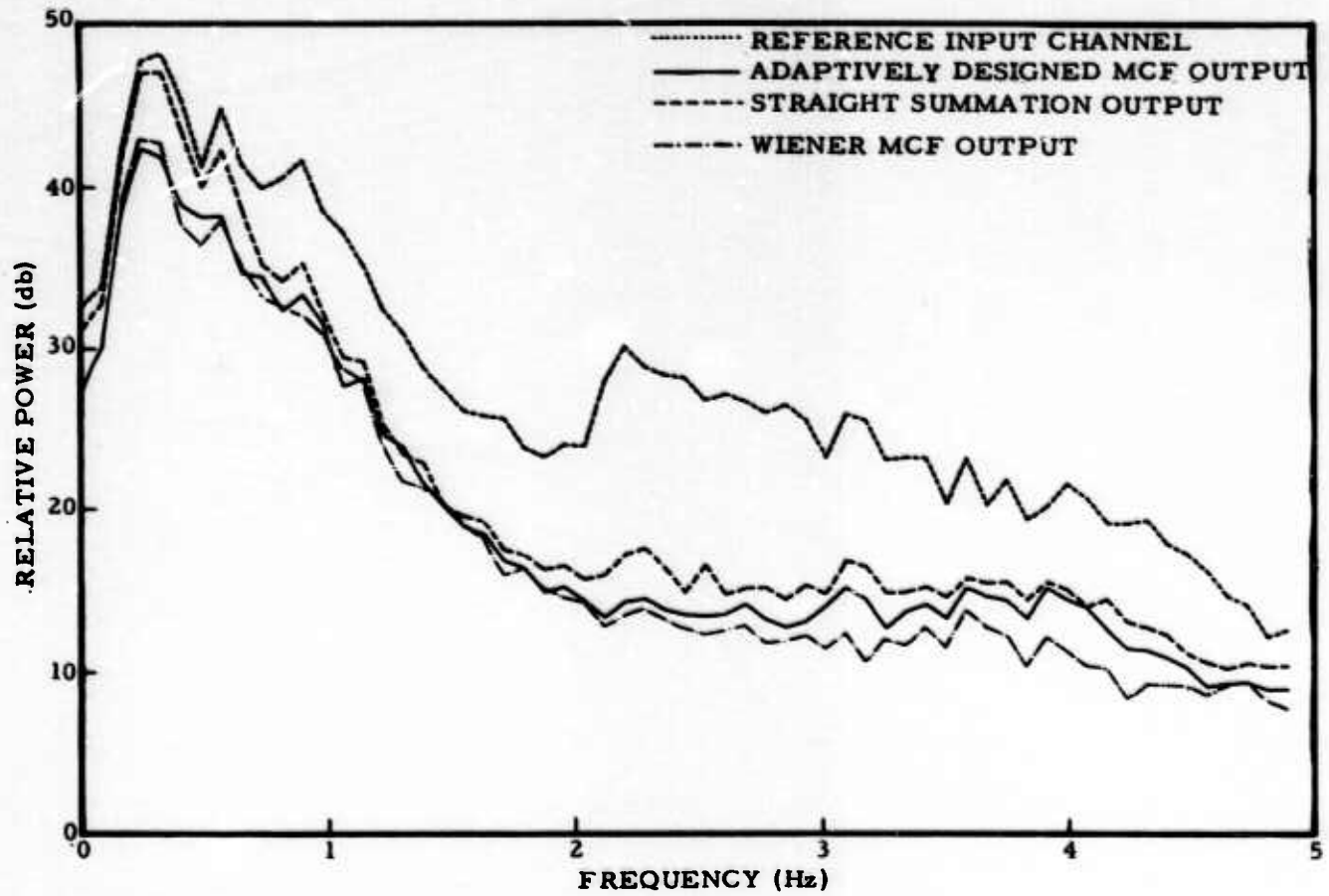

Figure 1. Output Noise Spectra from MCF Processing of Noise Sample 1010, Site 1

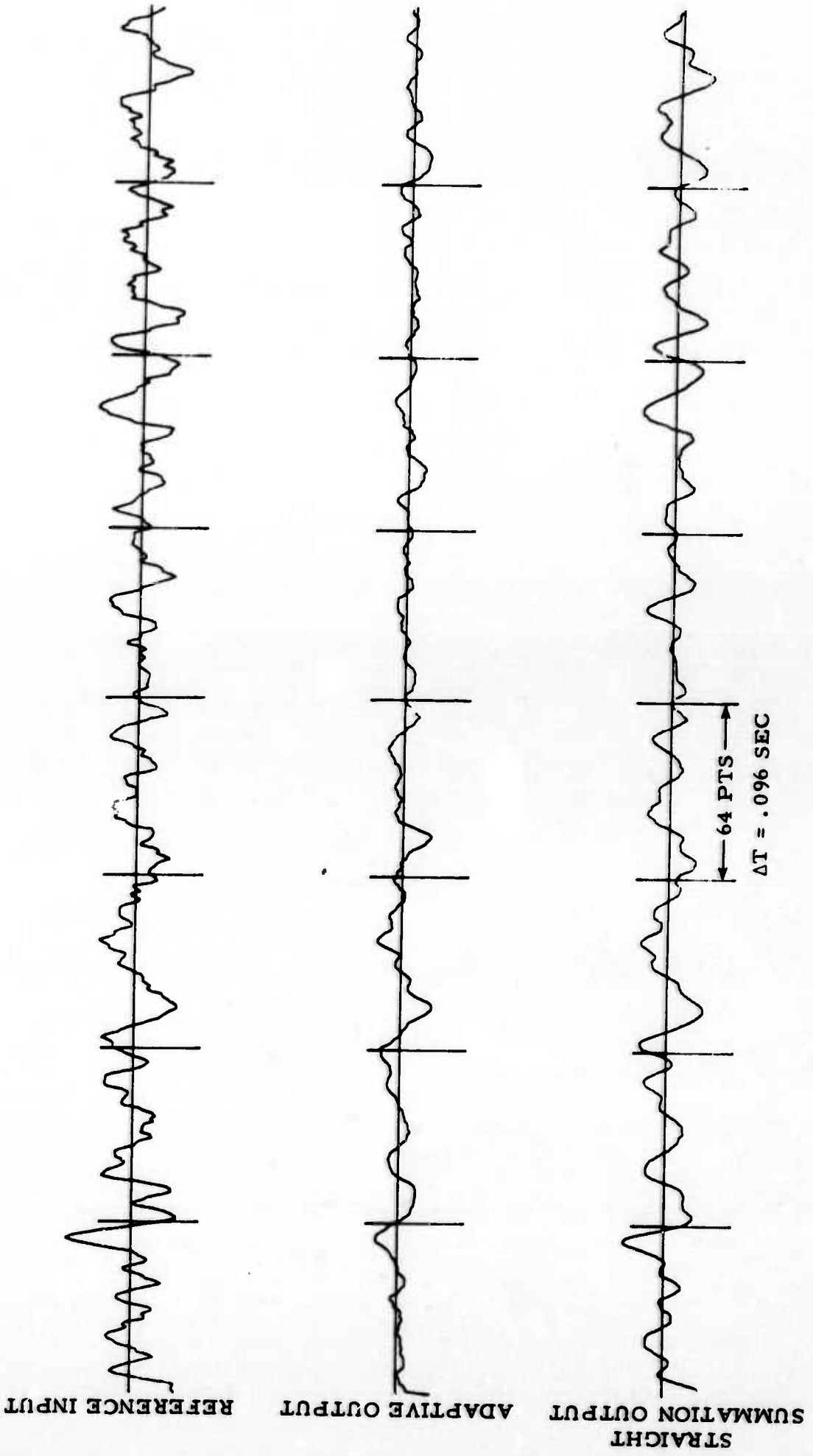

Figure 2. Adaptive Output Trace at a Convergence Rate of 0.25 of Maximum on Noise Sample 1010

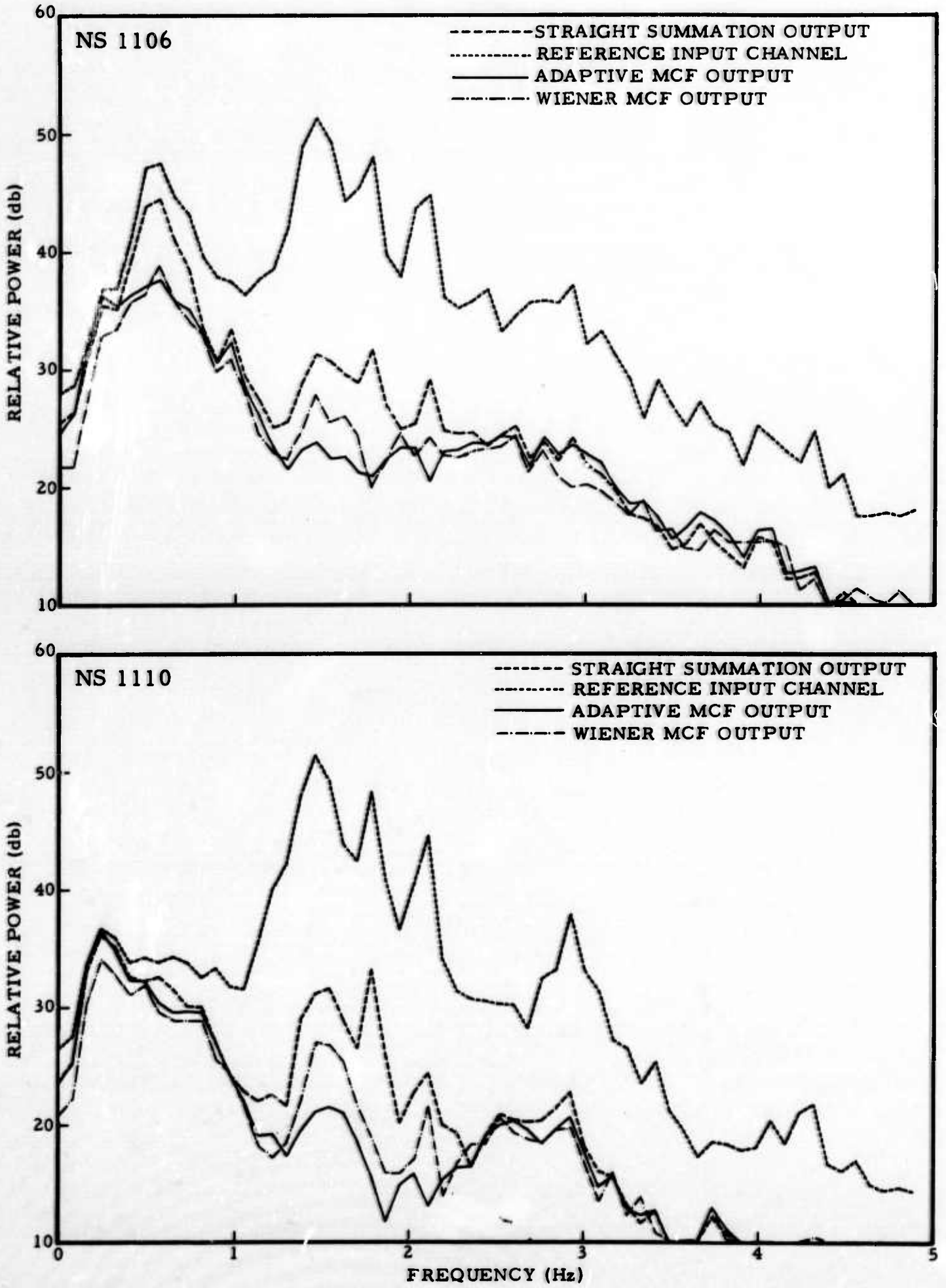

Figure 3. Spectral Comparison of Output Noise from Adaptive Processing of Noise Samples 1106 and 1110 of Site 2

Two attempts to adaptively design an MCF to be applied in a fixed mode resulted in an MCF which was inferior to the Wiener filters in the 1.46-Hz area. The first design consisted of adaptively processing the first segment of each of the 15 noise samples used in the Wiener design, starting with an adaption rate of 0.75 of maximum and exponentially decreasing it until a rate of 0.01 of maximum was used on the last segment processed. The second design was similar to the first except that the adaption rate was held constant at 0.25 of maximum over all 15 noise samples. The mean-square output during the adaptive processing for the two designs was computed every 65 points and plotted as shown in Figure 4. In Design 1, a large mean-square output shows the tendency of the adaptive process to become unstable at the high adaptive rate (0.75). However, after four to five noise samples, the mean-square output of the designs became very similar.

Applying the adaptively-designed MCFs as fixed filters to the same two noise samples previously processed with the Wiener MCF and adaptively provided very disappointing results near 1.46 Hz. Rejection in this area was equivalent to or less than that of the straight-summation process from which the adaptive design started (Figure 5).

Noise rejection in the other frequency bands is on the order of that obtained by the conventionally-designed Wiener MCF.

A filter was adaptively designed on a single noise sample at the 0.25 adaption rate and applied in a fixed mode to the same noise sample. During adaption the 1.46-Hz energy was rejected well, but during the fixed mode application, the 1.46-Hz energy out of the MCF was greater than that for the summation process. The use of lower adaption rates (0.05 to 0.005) to obtain fine tuning of the adaptive filtering resulted in a lower rejection capability of the 1.46-Hz noise during adaption and an output equivalent to that of the summation process during the fixed mode.

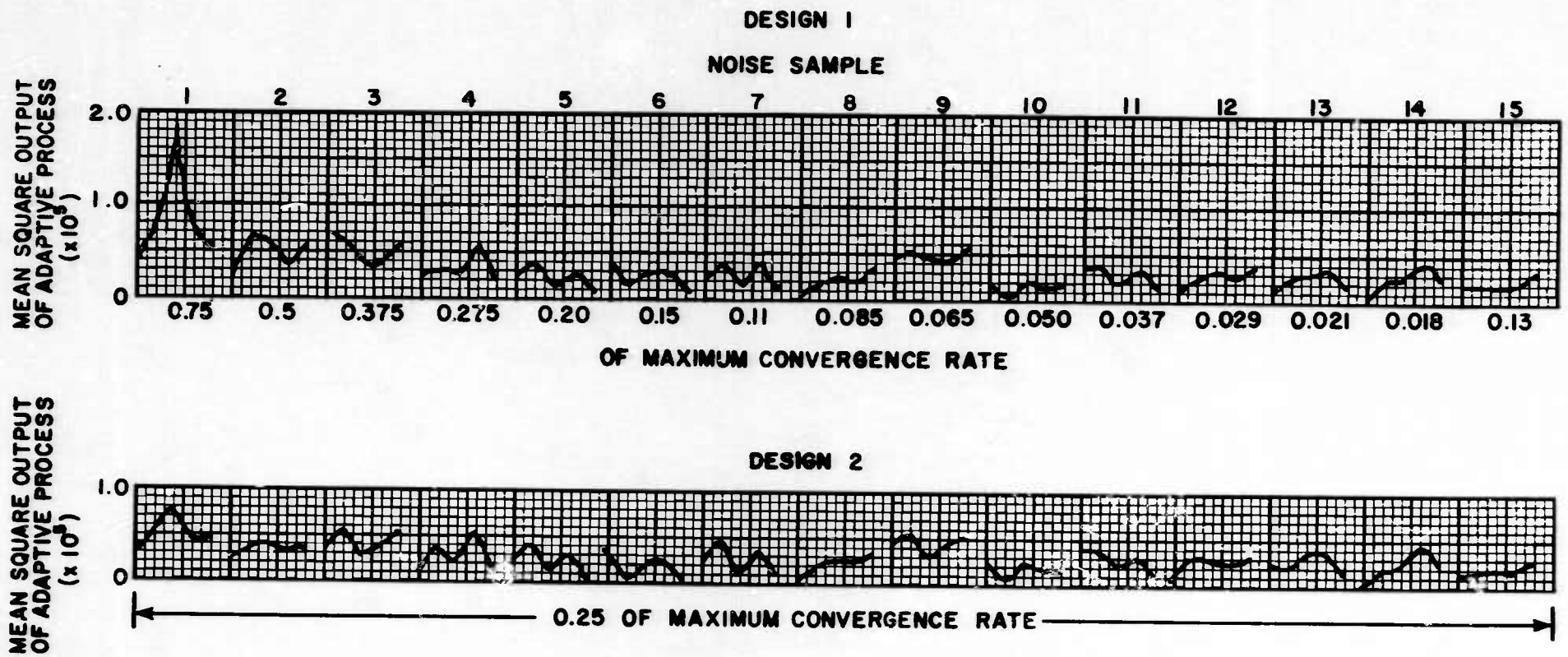

Figure 4. Mean-Square Output of Adaptive Process during MCF Design

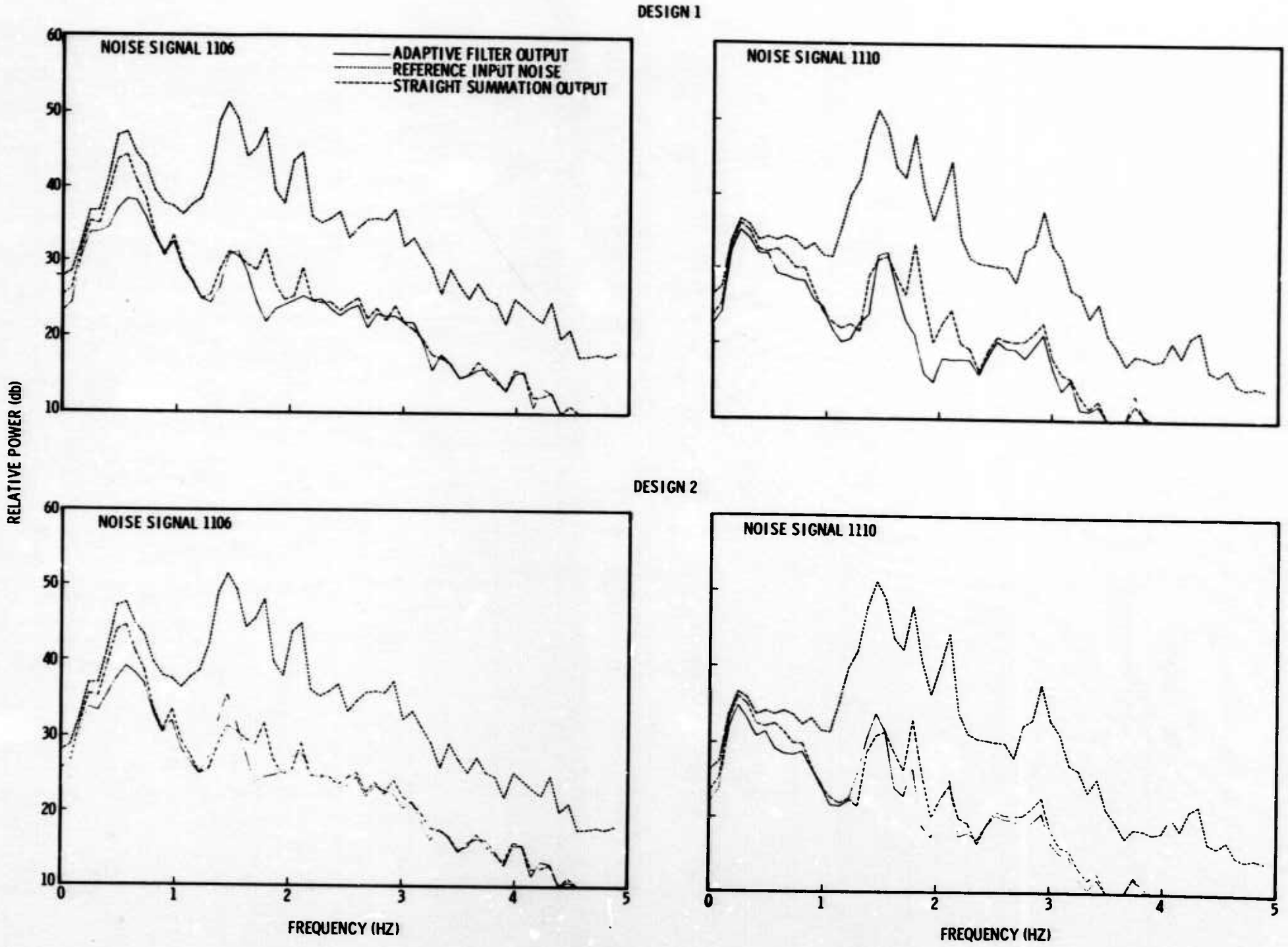

Figure 5. Output Noise Power-Density Spectra of Adaptively Designed MCFs during Fixed-Mode Processing

Based on these results it appears the energy in 1.46-Hz area is highly coherent and non-space stationary. An effective MCF to be designed adaptively and applied in a fixed mode would be very hard to obtain under these conditions. However, it appears that continuous on-line adaptive processing on this type of data would provide significant signal-to-noise improvement over any fixed MCF.

Site 3

The third array to be studied is also considered to have a very high ambient noise level. However, the high-frequency component of the noise field is both highly space and time stationary and is characterized by strong spectral spikes or lines. The five noise samples, from which the theoretical data were generated in the previous study to determine the convergence of time-domain adaptive filters for stationary data, were selected to further evaluate the adaptive design of MCFs.*

The optimum maximum-likelihood filters designed from the theoretical stationary data of the convergence rate study were applied to one of the ensemble noise samples (1014). The noise rejection obtained on the individual noise sample (Figure 6) is similar to that obtained on the theoretical data (Figure 7) from which it was designed.

The same noise sample (1014) was adaptively processed starting with a straight-summation process having two different adaption rates (0.05 and 0.25 of maximum). The noise rejection obtained by the adaptive process as shown in Figure 8 is somewhat less than the optimum maximum-likelihood filter; however, the results indicate that the adaptive filter is approaching the optimum filter in noise rejection, especially at the lower frequencies. Further investigation using various convergence rates and of various durations will be made to determine if the optimum filter is obtainable adaptively.

---

*Texas Instruments Incorporated, 1970: Convergence of Time-Domain Adaptive Maximum-Likelihood Filters for Stationary Data, Seismic Array Processing Techniques Tech. Rpt. 3, Contract F33657-70-C-0100, 26 Feb.

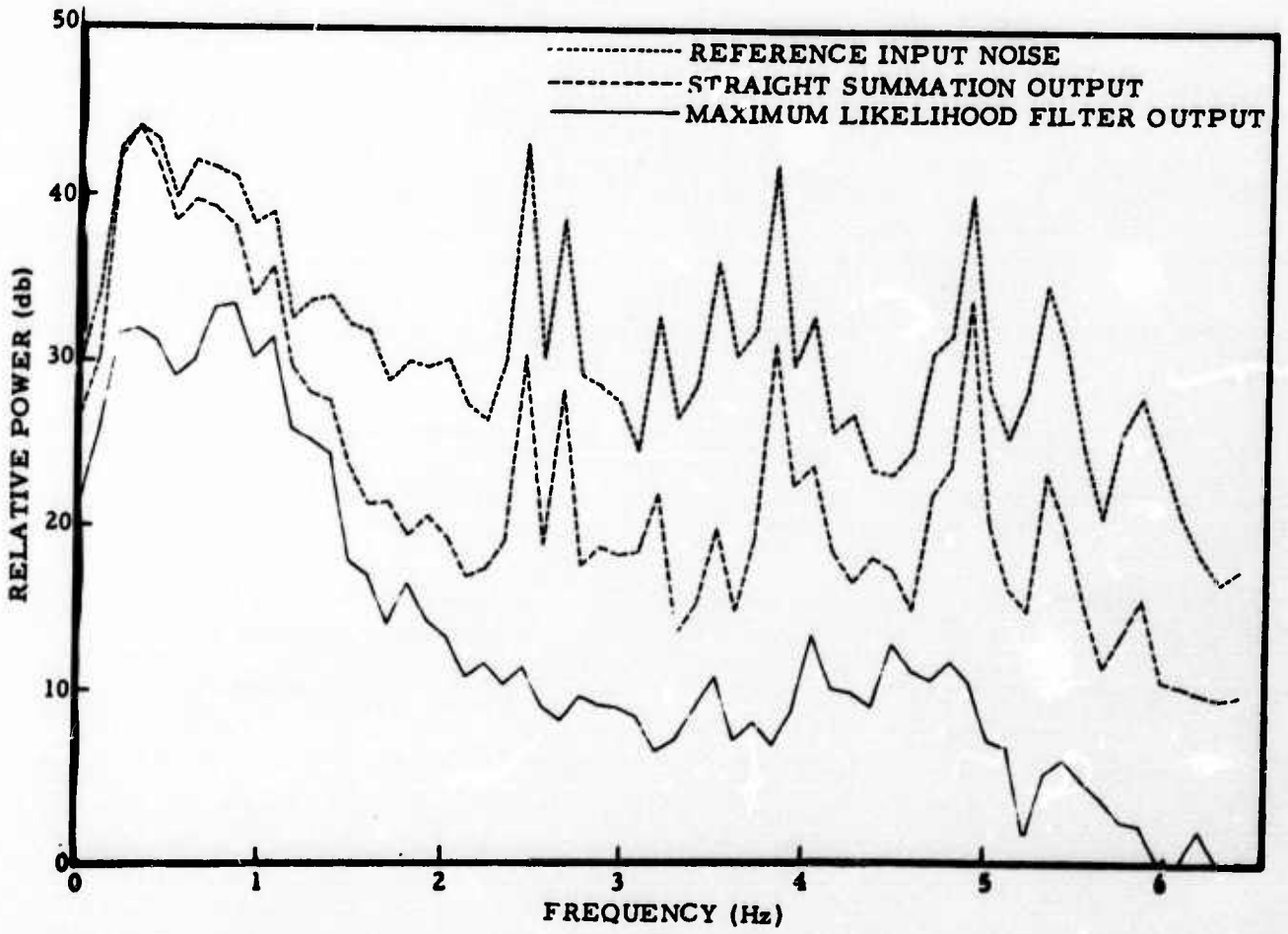

Figure 6. Output Power-Density Spectra of Optimum Maximum-Likelihood MCF Applied to Noise Sample 1014

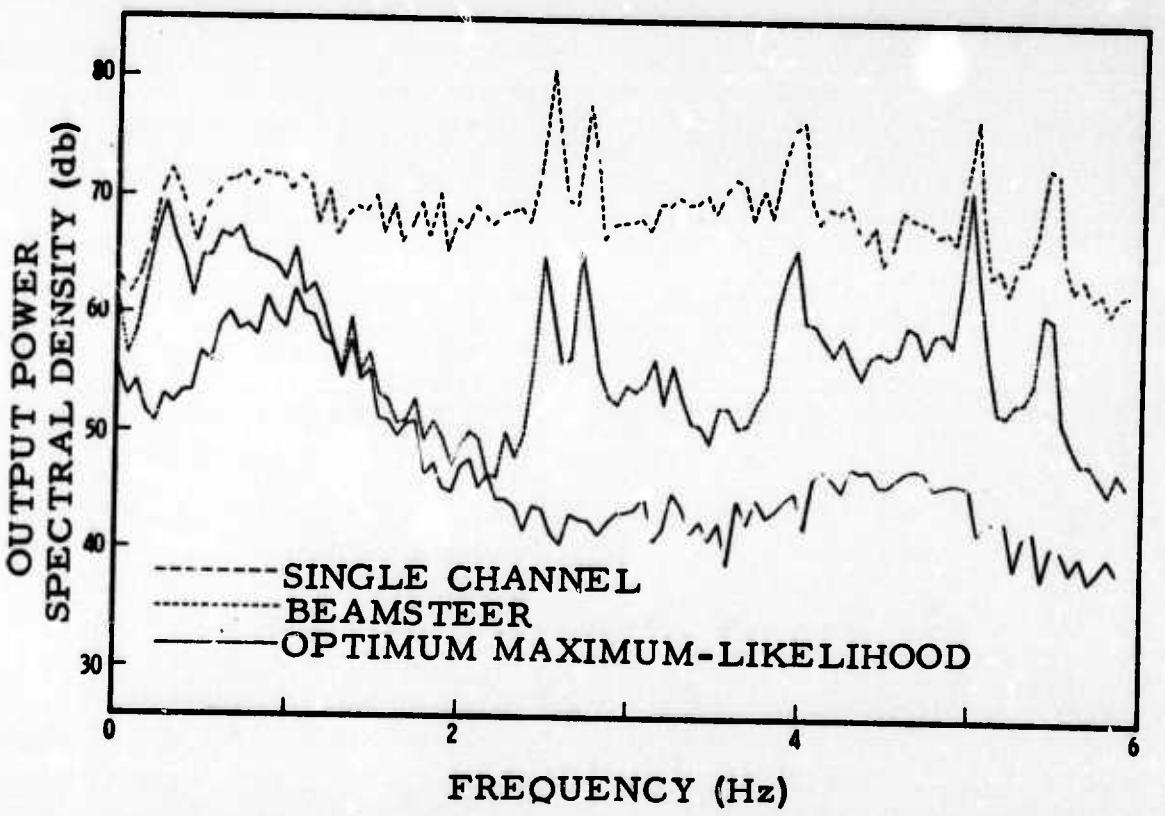

Figure 7. Output Power-Density Spectra of Optimum Maximum-Likelihood MCF Applied to Theoretical Ensemble Data

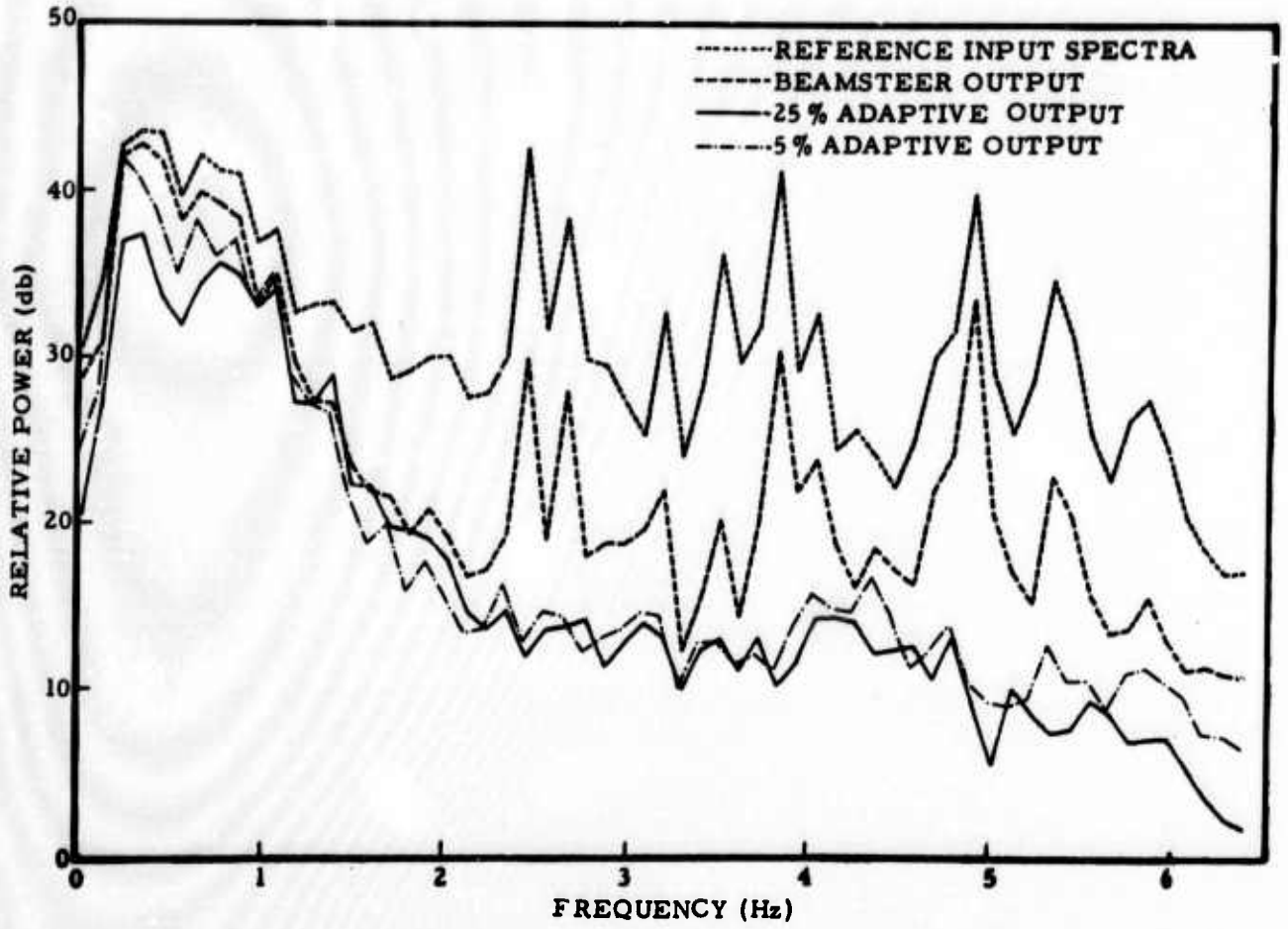

Figure 8. Comparison of Output Noise Power Density for Adaptive Filtering on Site 3 Data

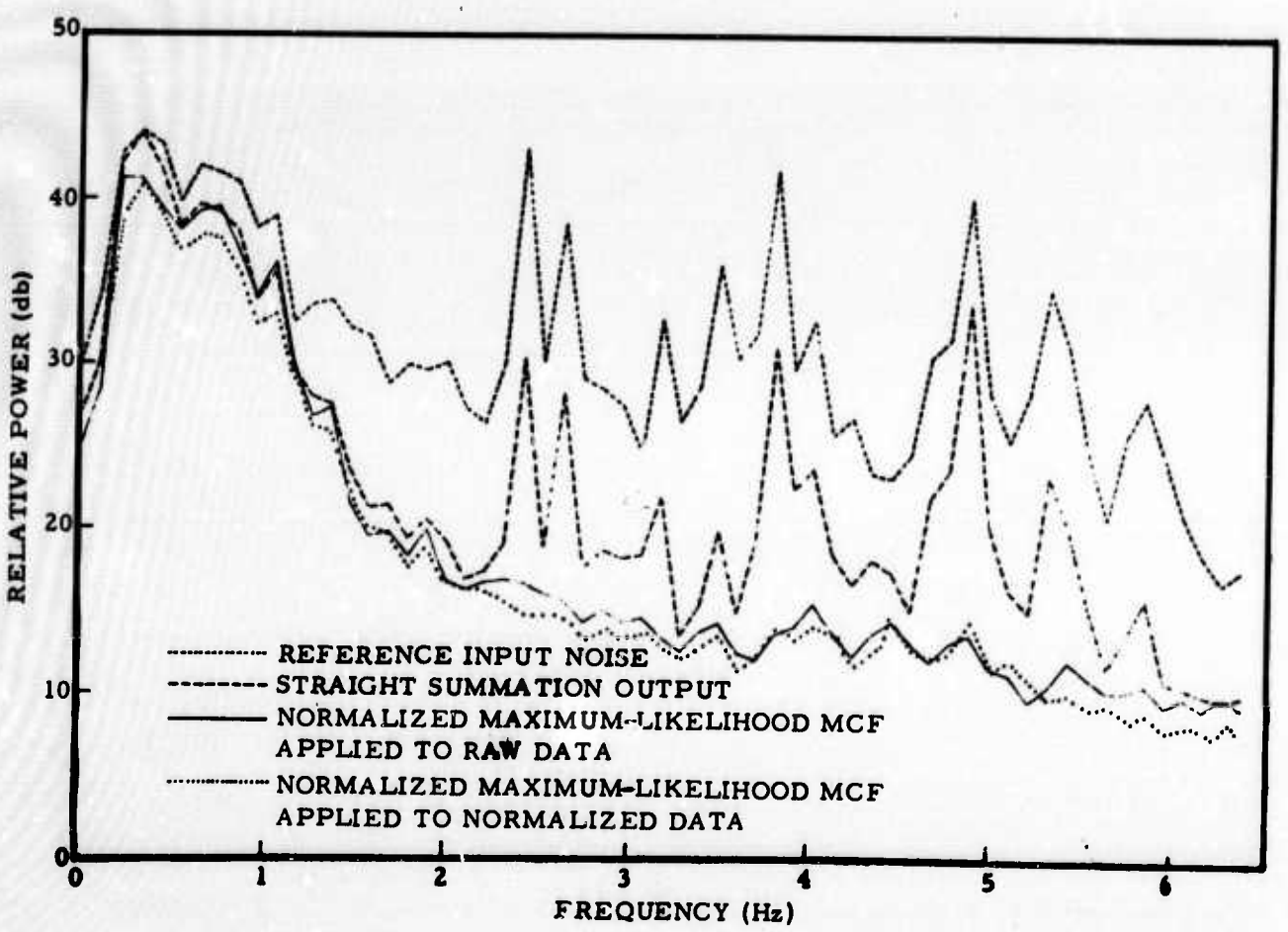

Figure 9. Spectral Evaluation of Noise Rejection Obtained by Maximum-Likelihood MCF Designed from Normalized Correlations

The noise rejection obtained by the previously discussed MCFs, especially at the lower frequencies, is suspected to be due in part to gain inequalities between array channels. Therefore, the optimum maximum-likelihood filters were redesigned from the correlations normalized to the total power on each channel. These normalized maximum-likelihood filters were then applied to noise sample 1014 both as recorded and as normalized by the factors used to normalize the correlation. The noise rejection in these two cases, as shown in Figure 9, is on the order of that previously obtained by adaptively processing the noise sample.

Additional efforts are being made to adaptively develop an MCF which will perform as well as the optimum maximum-likelihood filter using all five noise samples. A study is also being made on these data to determine the desirability of designing optimum MCFs in the frequency domain using conventional techniques. The effect of using various length transform gates to obtain the crosspower matrix for the MCF design will be determined. Three methods for obtaining the time-domain response of the MCF from the frequency-domain response will also be evaluated. These will include a straight inverse transform, a weighted mean-square estimate*, and the suboptimal multichannel technique.**

A comparison of the MCF designs discussed will be made on the basis of simplicity, computer capability and run time requirements, and the relative effectiveness of each method. The frequency-domain adaptive algorithm to be discussed in the next section will also be considered.

---

* Burg, John P., 1962: Weighted Mean Square Error Fit to a Given Frequency Response Using a Sampling Time Domain Operator, TI SSD Seismic Engineering Rpt 111-570001-16, Feb.

** Texas Instruments Incorporated, 1970: Suboptimal Multichannel Digital Filters, Seismic Array Processing Techniques Tech. Rpt. 2, Contract F33657-70-C-0100, 28 Jan.

B. MATHEMATICAL DEVELOPMENT OF FREQUENCY-DOMAIN MAXIMUM-LIKELIHOOD ADAPTIVE FILTERING ALGORITHM

The time domain maximum-likelihood adaptive filter is derived by minimizing the output y^t of a linear multichannel filter $\underline{f}$

$$y^t = \sum_{i=1}^{NC} \sum_{j=1}^{LF} f_{i,j}^t \, x_{i,t-j} = \underline{f}^T \underline{x}_t \tag{1}$$

subject to a system of constraints

where $$\underline{\underline{M}}\,\underline{f} = \underline{\alpha} \tag{2}$$

$\underline{x}_t$ is the input data vector

NC is the number of channels

LF is the length of filter

$$\underline{\underline{M}} = \left[\overbrace{\underline{\underline{I}} \; \underline{\underline{I}} \; \cdots \; \underline{\underline{I}}}\right] \tag{3}$$

$$\underline{\alpha} = (\alpha_1 \alpha_2 \cdots\cdots \alpha_{LF})^T, \quad \alpha_i = \delta_{i-s}, \quad s = LF/2$$

$\underline{\underline{I}}$ is a LF by LF identity matrix

The resulting adaptive algorithm is

$$\underline{f}^{t+1} = \underline{f}^t - B\, y^t \left[\underline{\underline{I}} - \frac{1}{NC}\,\underline{\underline{U}}\right] \underline{x}_t \tag{4}$$

where $\underline{\underline{I}}$ is a LF x NC by LF x NC identity matrix, $\underline{\underline{U}}$ is a square matrix with all elements equal to 1 and dimension LF x NC, and B is a convergent parameter.

Here we derive a similar adaptive algorithm in the frequency domain.

If we take the Fourier transformation of each channel of the input data and time domain filter, and let

$$X^{t}_{i,k} = \sum_{r=0}^{LF-1} x_{i,t-r-1}\, e^{-j2\pi k r/LF} \tag{5}$$

$$F^{t}_{i,k} = \sum_{r=0}^{LF-1} f^{t}_{i,r+1}\, e^{-j\pi k r/LF} \tag{6}$$

where

$$k = 0,\ 1,\ 2,\ \text{----------},\ LF-1$$

$$i = 1,\ 2,\ 3,\ \text{----------},\ NC$$

then, according to Parseval's theorem, we have

$$\sum_{j=1}^{LF} f^{t}_{i,j}\, x_{i,t-j} = \frac{1}{LF} \sum_{k=0}^{LF-1} F^{t}_{i,k}\, X^{t\,*}_{i,k} \tag{7}$$

where * means complex conjugate.

Thus, Equation 1 can be written as

$$y^{t} = \frac{1}{LF} \sum_{i=1}^{NC} \sum_{k=0}^{LF-1} F^{t}_{i,k}\, X^{t\,*}_{i,k} = \sum_{k=0}^{LF-1} y^{t}_{k} \tag{8}$$

where

$$y^{t}_{k} = \frac{1}{LF} \sum_{i=1}^{NC} F^{t}_{i,k}\, X^{t\,*}_{i,k} \tag{9}$$

Let the Fourier transform (transform each row separately) of $\underline{\underline{I}}$ in Equation 3 be $\underline{\underline{N}}'$.

where

$$\underline{\underline{N}}' = \begin{bmatrix} R_{1,0} & R_{1,1} & \cdots\cdots & R_{1,LF-1} \\ R_{2,0} & R_{2,1} & \cdots\cdots & R_{2,LF-1} \\ \vdots & & & \vdots \\ R_{LF,0} & R_{LF,1} & \cdots\cdots & R_{LF,LF-1} \end{bmatrix}$$

and

$$\underline{\underline{N}} = \overbrace{\left[\underline{\underline{N}}' \; \underline{\underline{N}}' \; \cdots \; \underline{\underline{N}}'\right]}^{NC}$$

Then, Equation 2 can be written as

$$\frac{1}{LF} \; (\underline{\underline{N}}^{*} \; \underline{F}) = \underline{\alpha} \quad \text{or} \quad \underline{\underline{N}}^{*} \; \underline{F} = \underline{\beta}$$

where

$$\underline{\beta} = LF \; \underline{\alpha}$$

We assume that all frequency components of y^t are independent, i.e., y_k^t's are independent. Then $(y^t)^2$ may be minimized by minimizing each $|y_k^t|^2$ independently; i.e., we may minimize $y_k^t \; y_k^{t*}$ subject to the constraint

$$\underline{\underline{\tilde{N}}}_k^{*} \; \tilde{F}_k = \underline{\beta}_k \tag{10}$$

where

$$\underline{\beta}_k = (\beta_{1,k}^R \quad \beta_{1,k}^I \; \cdots\cdots \; \beta_{LF,k}^R \quad \beta_{LF,k}^I)^T$$

$$\sum_{k=0}^{LF-1} \beta_{i,k}^R = LF \; \alpha_i$$

$$\sum_{k=0}^{LF-1} \beta_{i,k}^I = 0$$

$$\underset{\sim}{F}_k = (F^R_{1,k}, iF^R_{1,k} \text{ ---------- } F^R_{NC,k}, iF^I_{NC,k})^T$$

$$\underset{\sim}{N}_k = \underbrace{\begin{bmatrix} R_{1,k} & 0 & R_{1,k} & 0 & \text{----------} & R_{1,k} & 0 \\ 0 & R_{1,k} & 0 & R_{1,k} & \text{----------} & 0 & R_{1,k} \\ R_{LF,k} & 0 & R_{LF,k} & 0 & \text{----------} & R_{LF,k} & 0 \\ 0 & R_{LF,k} & 0 & R_{LF,k} & \text{--------} & 0 & R_{LF,k} \end{bmatrix}}_{2\,NC}$$

$F^R_{i,j}$ and $F^I_{i,j}$ are the real and imaginary part of $F_{i,j}$, respectively. Let

$$\Phi_k = y^t_k y^{t^*}_k + 2\,(\underset{\sim}{\underset{\sim}{N}}^*_k \underset{\sim}{F}_k - \underset{\sim}{\beta}_k)^T \underset{\sim}{\lambda}_k$$

and

$$\nabla_k = \left[\frac{\partial}{\partial F^R_{1,k}}, i\frac{\partial}{\partial F^I_{1,k}}, \text{----------}, \frac{\partial}{\partial F^R_{NC,k}}, i\frac{\partial}{\partial F^I_{NC,k}} \right]^T$$

Then

$$\nabla_k \Phi_k = 2(\underset{\sim}{\psi}_k + \underset{\sim}{\underset{\sim}{N}}^{*T}_k \underset{\sim}{\lambda}_k) \qquad (11)$$

where

$$\underset{\sim}{\psi}_k = \frac{1}{LF} \begin{bmatrix} \text{Re}\left[y^t_k X^t_{1,k}\right] \\ i\,\text{Im}\left[y^t_k X^t_{1,k}\right] \\ \vdots \\ \text{Re}\left[y^t_k X^t_{NC,k}\right] \\ i\,\text{Im}\left[y^t_k X^t_{NC,k}\right] \end{bmatrix}$$

Re and Im represents "the real part of" and "the imaginary part of".

In order to find the Langrangian multiplier $\underline{\lambda}_k$, let $\nabla_k \Phi_k = 0$. Then we have

$$\underline{\lambda}_k = -\left[\underset{=}{\tilde{N}}^*_k \; \underset{=}{\tilde{N}}^{*T}_k\right]^{-1} \underset{=}{\tilde{N}}^*_k \; \underline{\psi}_k \tag{12}$$

Substituting Equation 12 into Equation 11, we have

$$\nabla_k \Phi_k = 2\left\{\underline{\underline{I}} - \underset{=}{\tilde{N}}^{*T}_k \left[\underset{=}{\tilde{N}}^*_k \; \underset{=}{\tilde{N}}^{*T}_k\right]^{-1} \underset{=}{\tilde{N}}^*_k\right\} \underline{\psi}_k \tag{13}$$

After removing the redundant rows of $\underset{=}{\tilde{N}}^*_k$, we have

$$\underline{N}^*_k = R^*_{1,k} \begin{bmatrix} \overbrace{1\;0\;1\;0\;-\;-\;-\;-\;-\;-\;1\;0}^{2\,NC} \\ 0\;1\;0\;1\;-\;-\;-\;-\;-\;-\;0\;1 \end{bmatrix}$$

Thus,

$$\underset{=}{\tilde{N}}^{*T}_k \left[\underset{=}{\tilde{N}}^*_k \; \underset{=}{\tilde{N}}^{*T}_k\right]^{-1} \underset{=}{\tilde{N}}^*_k = \frac{1}{NC}$$

$$\overbrace{\begin{bmatrix} 1\;0\;1\;0\;-\;-\;-\;-\;-\;-\;1\;0 \\ 0\;1\;0\;1\;-\;-\;-\;-\;-\;-\;0\;1 \\ \vdots\;\vdots\;\vdots\;\vdots \\ \vdots\;\vdots\;\vdots\;\vdots \\ \vdots\;\vdots\;\vdots\;\vdots \\ \vdots\;\vdots\;\vdots\;\vdots \\ \vdots\;\vdots\;\vdots\;\vdots \\ 1\;0\;1\;0\;-\;-\;-\;-\;-\;-\;1\;0 \\ 0\;1\;0\;1\;-\;-\;-\;-\;-\;-\;0\;1 \end{bmatrix}}^{2\,NC} \Bigg\} 2\,NC$$

and Equation 13 becomes

$$\nabla_k \Phi_k = 2\left\{ \underline{\underline{I}} - \frac{1}{NC} \overbrace{\begin{bmatrix} 1 & 0 & 1 & 0 & & 1 & 0 \\ 0 & 1 & 0 & 1 & & 0 & 1 \\ \vdots & & & & & & \\ 1 & 0 & 1 & 0 & & 1 & 0 \\ 0 & 1 & 0 & 1 & & 0 & 1 \end{bmatrix}}^{2\,NC} \right\} \underline{\psi}_k$$

$$= - \frac{2}{NC} \underline{\underline{P}}\, \underline{\psi}_k$$

where

$$\underline{\underline{P}} = \overbrace{\begin{bmatrix} 1\text{-}NC & 0 & 1 & 0 & \cdots & 1 & 0 \\ 0 & 1\text{-}NC & 0 & 1 & & 0 & 1 \\ 1 & 0 & 1\text{-}NC & 0 & \cdots & 1 & 0 \\ \vdots & \vdots & \vdots & \vdots & & \vdots & \vdots \\ 0 & 1 & 0 & 1 & \cdots & 0 & 1\text{-}NC \end{bmatrix}}^{2\,NC}$$

The adaptive algorithm can be written as

$$\underline{\tilde{F}}_k^{t+1} = \underline{\tilde{F}}_k^{t} + \frac{2\,B_k}{NC}\, \underline{\underline{P}}\, \underline{\psi}_k \qquad (14)$$

or

$$F_{i,k}^{t+1} = F_{i,k}^{t} + \frac{2\,B_k}{LF}\; y_k^t \left[\overline{X}_k^t - X_{i,k}^t\right] \qquad (15)$$

where

$$\overline{X}_k^t = \frac{1}{NC} \sum_{i=1}^{NC} X_{i,k}^t$$

Since $y_k^t = y_{LF-k}^{t*}$ and y_0^t is real, we can write Equation 8 as

$$y^t = y_0^t + 2\,\mathrm{Re}\left[\sum_{k=1}^{LF/2} y_k^t\right] \qquad (16)$$

Since $F_{i,k}^t = F_{i,LF-k}^{t*}$ and $F_{i,0}^t$ is real, we only need to calculate Equation 15 for k = 0, 1, ------ , LF/2.

We plan to use the algorithm derived as above to run one set of synthetic data and one set of real data and compare the results with the time-domain maximum-likelihood adaptive filter.

C. FREQUENCY-DOMAIN ADAPTIVE MCF DESIGN AND PROCESSING

The frequency-domain adaptive algorithm (derived in the previous discussion) has been programmed and checked out by a limited amount of processing. A study to determine the proper convergence factor for each frequency is being conducted currently.

Initially, the theoretical stationary data, developed and used during the convergence study of time-domain adaptive maximum-likelihood filters, will be processed using the derived frequency-domain algorithm and compared to the time-domain results. If satisfactory results are obtained, some of the measured data being used in the MCF adaptive design study will be processed by the algorithm for additional comparisons to similar time-domain processing.

SECTION III: ON-LINE ADAPTIVE MULTICHANNEL PROCESSING

The objective of the on-line adaptive processing task is to evaluate adaptive filtering and associated problems in a real-time processing mode. This includes the investigation and implementation of procedures for handling the various problems which would normally be encountered during continuous on-line processing.

A set of specifications has been developed for an on-line program to perform the continuous processing of the ALPA data arriving at the SAAC. The specifications have been discussed with the programmer and modified, based on computing capabilities available at the SAAC. The resulting program should have adequate flexibility to allow for full investigation and handling of the problems previously presented in Quarterly Report No. 1 Programming of the software should be completed during the latter part of March, at which time adequate data from ALPA should be available for processing.

To support the on-line adaptive processing tasks, the capability to read raw data from the ALPA as recorded at SAAC is being developed in Dallas for the Texas Instruments' IBM 360 system. Being prepared are analysis packages to perform supplemental processing on the data as needed to fully evaluate the on-line adaptive processing.

Some preliminary analysis is being conducted on the data previously discussed in the adaptive MCF design study in an effort to establish the initial parameters to be used in the on-line processing. A study using the Site 2 data has been conducted to determine the effects of adapting less frequently. Results are summarized in Table 1. Threshold levels for freezing the adaption of the filters under possible signal conditions are also being analyzed.

Table 1

MCF NOISE REJECTION (SITE 2 DATA)

TYPE OF MULTICHANNEL PROCESSING	NOISE IN/NOISE OUT MS POWER (db)			
	.25-1.0 Hz		1.0-3.0 Hz	
	NS 1106	NS 1110	NS 1106	NS 1110
Straight Beamsteering	3.3	2.6	16.6	16.4
Wiener Filtering	8.3	4.1	20.1	22.2
Adaptive Processing (updating every point)	7.9	3.3	20.5	24.7
Adaptive Processing (updating every second point)	7.9	3.4	19.5	23.3
Adaptive Processing (updating every third point)	7.8	3.5	18.6	22.1
Adaptive Processing (updating every fifth point)	7.5	3.3	15.3	19.0
Input Level (db)	52.8	43.6	57.4	56.9

SECTION IV: LONG-PERIOD ARRAY DATA ANALYSIS

A. MATCHED-FILTERING STUDY

A matched-filtering study has been done using LASA beam outputs of 17 Rayleigh wavetrains from shallow events in the Kurile-Kamchatka area. Matched filtering of each event was done using some master events from the region, a chirp signal, and wavetrains generated from crustal models found in the literature.

The more important tentative conclusions are as follows:

- A nearby (less than 200 km) master event appears to be the best matched filter
- It appears that a master event within about 200 km of the test event is necessary to have a high confidence that matched filtering will give any signal-to-noise improvement over a tight bandpass filter
- Matched filter gains in signal-to-noise improvement (as compared to bandpass filtering), even using close master events, are small for this data (generally between 0 and 3 db)

A special technical report covering the details of this study will be submitted during March.

B. NEPENTHE STUDY

This task investigates the NEPENTHE* technique by means of a controlled experiment. The NEPENTHE process computes a series of Fourier amplitude spectra from a sequential series of noise samples. The upper 90-percent limit of the noise spectra is estimated using the chi-squared distribution

---

* Simons R.S., W.R. Weber, and H.S. Travis, 1968: Preliminary Report on a Single Channel Statistical Technique for Suppressing Long-Period Micro-Seismic Noise, Geotech Tech Rpt. 68-25, Contract F33657-68-C-0734, Project VT-8703, 19 July.

and these spectra are subtracted from a subsequent spectra sample. The resultant spectra, with negative values set equal to zero, are inverse transformed and the time-domain result is displayed. The process then moves ahead one sample and is repeated.

A 128-min long-period noise sample from TFO was used to estimate the upper 90-percent limit of the noise spectra. A Rayleigh-wave signal has been added to this noise sample at signal-to-noise-ratios of 1:1, 2:1, 4:1, and 1:2.

Initially both the NEPENTHE technique and a bandpass filter (0.017 to 0.1 Hz passband) will be output. These will be compared with the known signal to see how good a signal estimate is obtained in the presence of the noise.

C. TFO AND UBO NOISE ANALYSIS

High-resolution maximum-entropy power density spectra have been computed for two TFO long-period noise samples and for three UBO long-period noise samples. These spectra are shown in Figures 10 through 14. All channels, except wild or dead ones, have been included. In the case of the UBO data, the vertical scales for the spectra are given in units of db relative to 1 $(m\mu)^2$/Hz. The calibration information for the UBO seismometers was supplied by Seismic Data Laboratories.

These spectra show the general characteristics previously observed in the spectra of long-period seismic noise—in particular, the peaks in the vicinities of 0.06 Hz and 0.13 Hz, and the trough at 0.09 Hz. However, the UBO spectra do not appear to exhibit as great a negative slope of power versus frequency as is generally observed in the spectra of long-period noise.

Several of the TFO spectra show fairly prominent spikes, e.g., the peak at 0.013 Hz in the spectrum of the north-south seismometer of LP2 in the first noise sample and at 0.03 Hz for the same instrument in the second

noise sample. All of these apparently anomalous peaks occur below 0.05 Hz and are therefore unlikely to be of seismic origin.

The rms noise levels in millimicrons for the data intervals over which the spectra were computed is given for the UBO data in Table 2.

Table 2

RMS NOISE LEVELS FOR UBO
NOISE SAMPLES (in mμ)

Location	LPZ	LPN	LPE
	First Sample		
LP1	28.4	——	——
LP2	19.6	——	——
LP3	17.8	——	——
LP4	12.9	——	10.3
LP5	23.4	26.3	26.3
LP6	26.1	23.1	25.6
LP7	——		
	Second Sample		
LP1	28.8	——	——
LP2	19.1	——	——
LP3	19.0	——	——
LP4	13.1	——	——
LP5	22.9	——	——
LP6	24.3	——	——
LP7	——	——	25.4
	Third Sample		
LP1	30.1	——	——
LP2	19.7	23.0	19.4
LP3	17.7	——	18.5
LP4	——	——	10.3
LP5	22.5	24.7	26.4
LP6	22.5	20.1	——
LP7	24.6	20.3	22.7

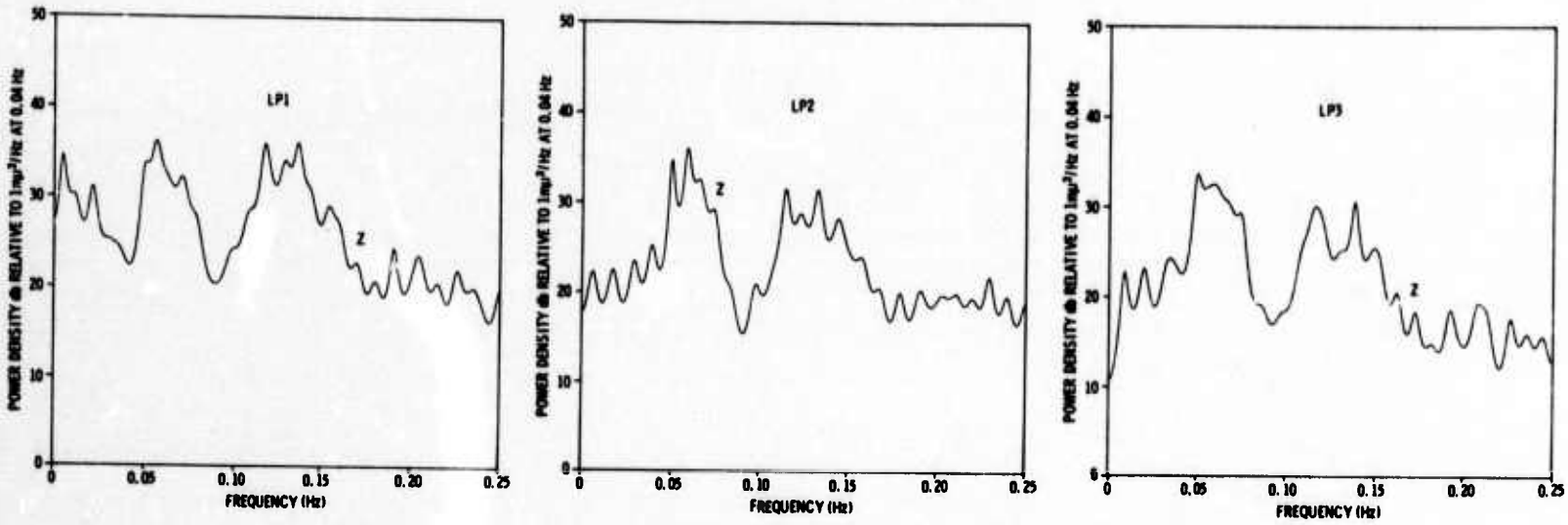

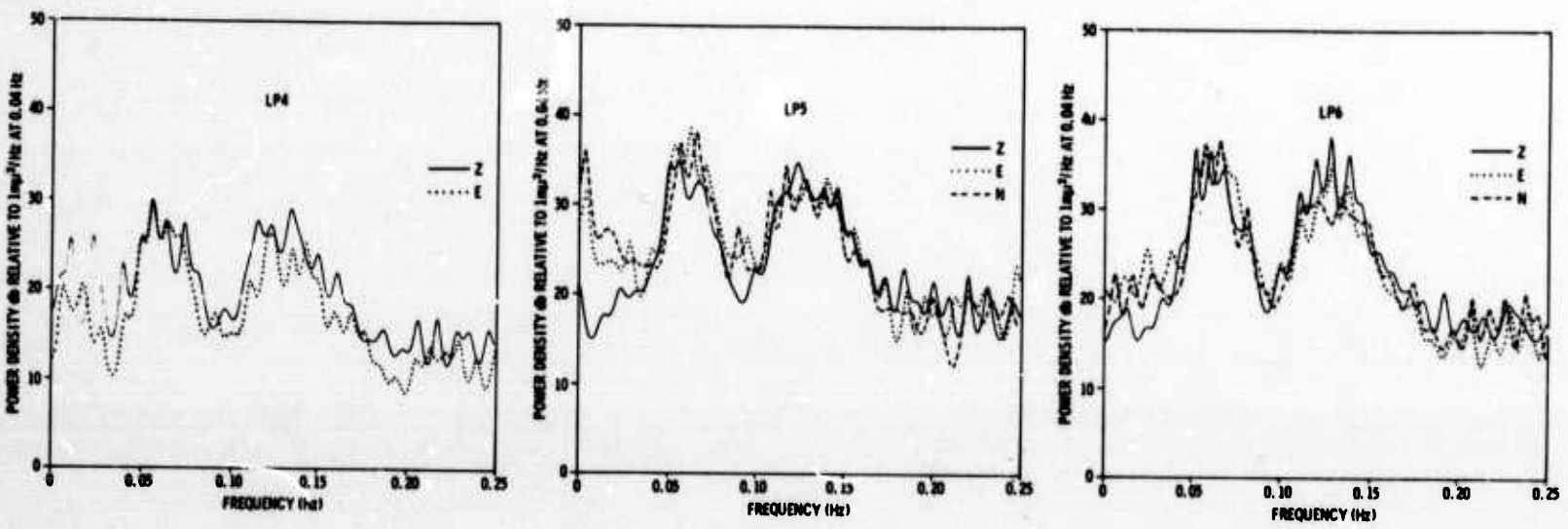

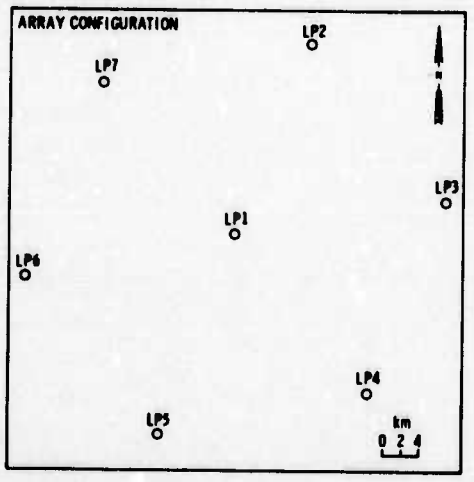

Figure 10. Power Spectra of Noise Sample Beginning at 1224Z, 27 July 1969 (UBO)

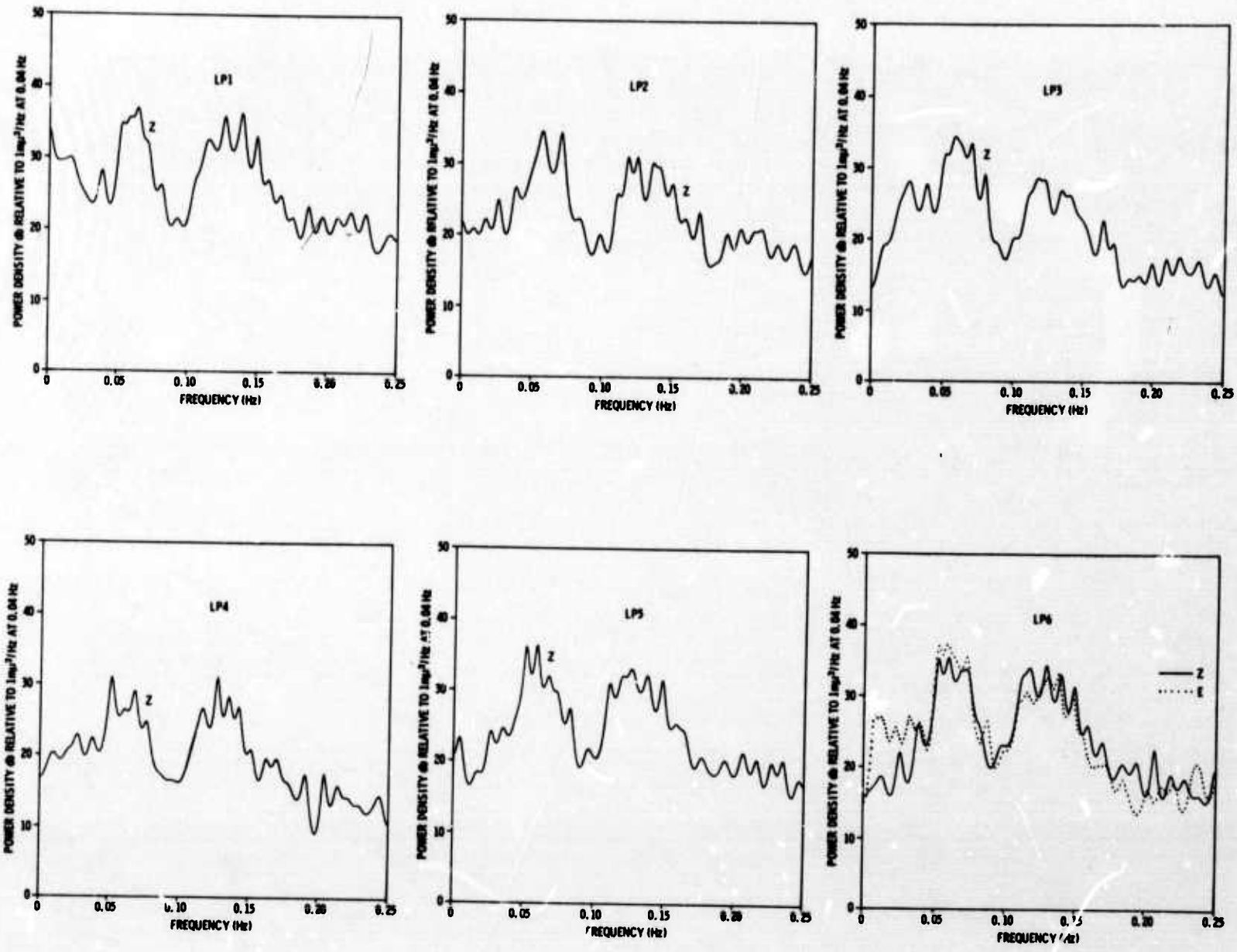

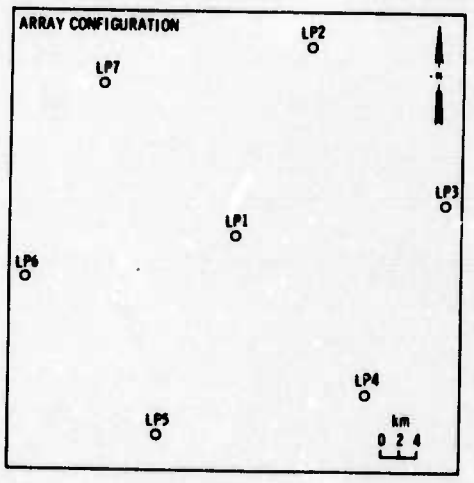

Figure 11. Power Spectra of Noise Sample Beginning at 1800Z, 27 July 1969 (UBO)

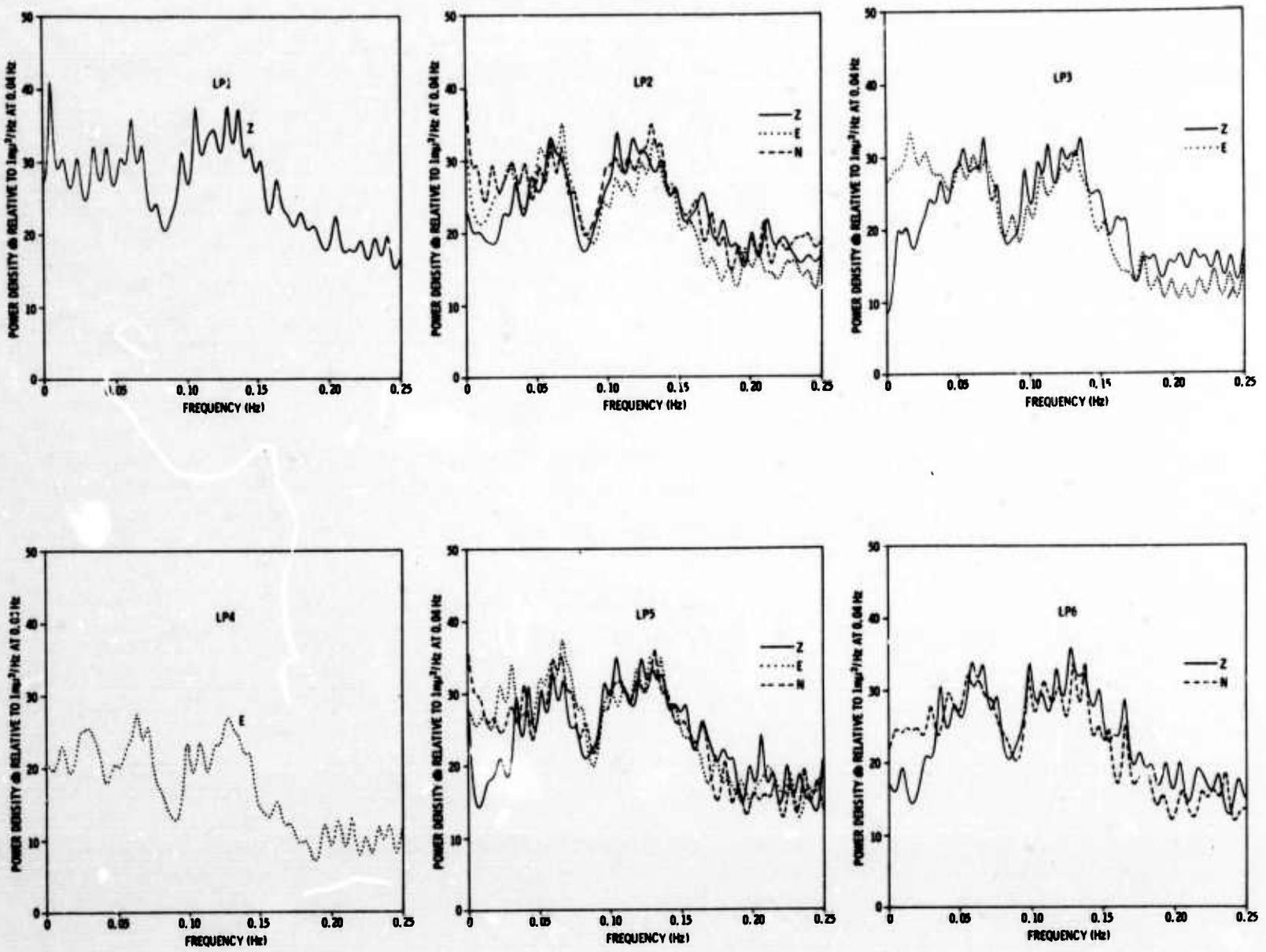

Figure 12. Power Spectra of Noise Sample Beginning at 1227Z, 30 July 1969 (UBO)

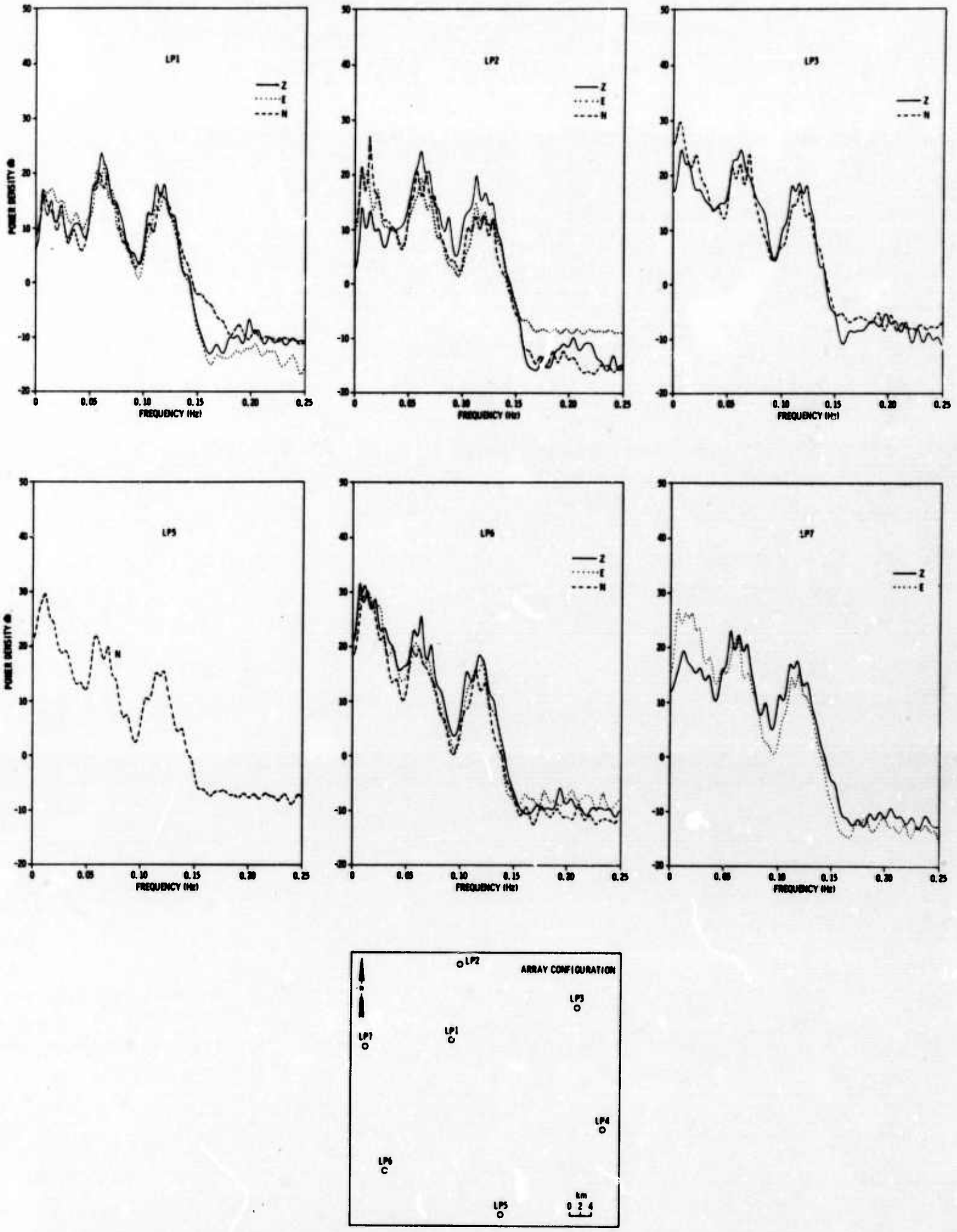

Figure 13. Power Spectra of Noise Sample Beginning at 0650Z, 21 February 1969 (TFO)

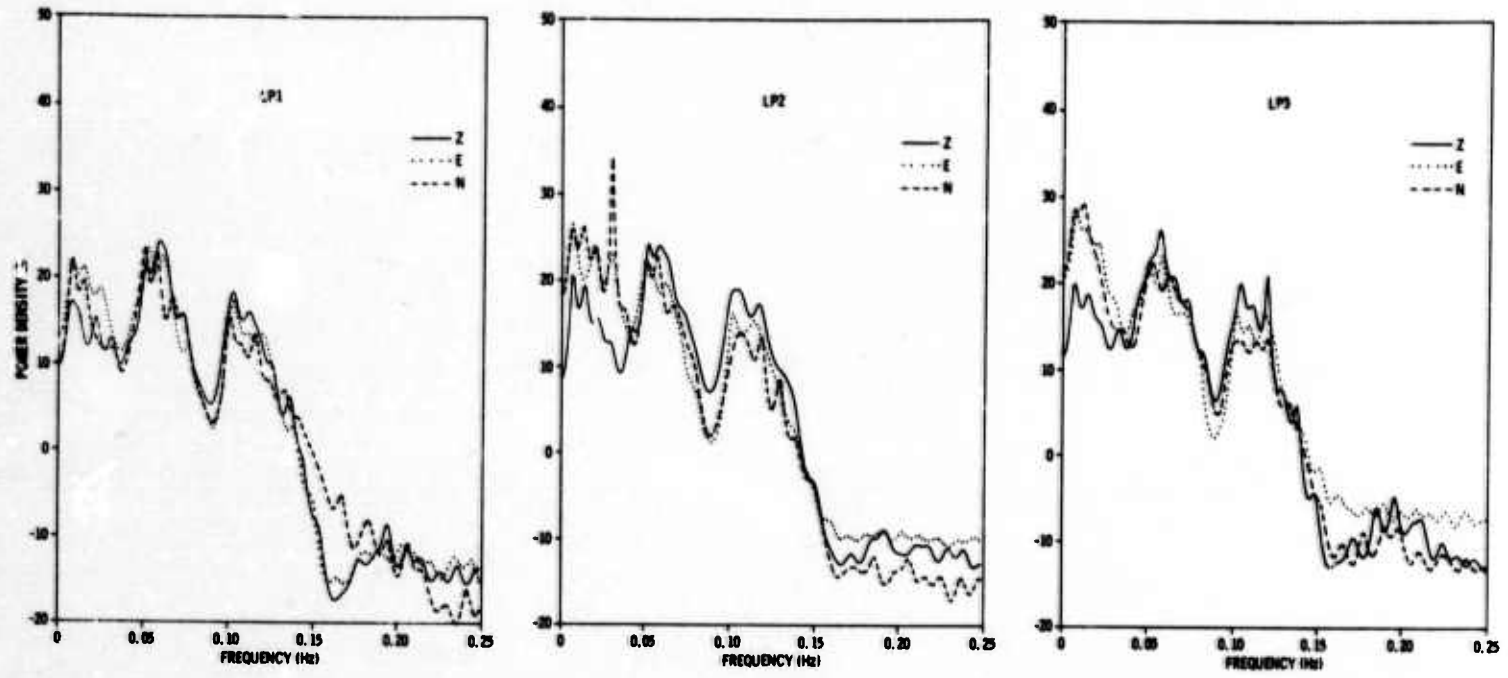

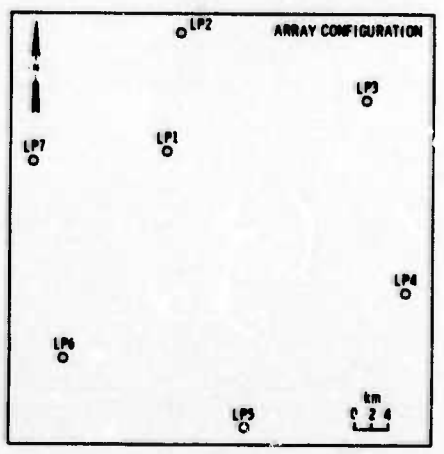

Figure 14. Power Spectra of Noise Sample Beginning at 0250Z, 1 March 1969 (TFO)

SECTION V: TFO EXTENDED SHORT-PERIOD ARRAY NOISE STUDY

An ambient noise sample was selected from two recording periods, 6 June to 21 June 1968, designated as the "summer" noise, and 27 January to 4 March 1969, designated as the "winter" noise. The objective is to compare the summer and winter noise field characteristics, to estimate the time and space stationarity of these noise fields, and to establish the effectiveness of multichannel processing of the extended array.

The summer data have been processed and in the previous quarterly report an initial analysis of the data was presented which indicated possible problems in the data. Investigation into the processing revealed that approximately half of the elements were reversed in polarity during recording. A similar investigation of the winter data revealed that this problem also exists with the winter data. Corrections were made to the crosspower matrices which had been computed for each noise sample.

A. SUMMER NOISE ANALYSIS

The spatial organization of the coherent noise field for the summer noise sample was analyzed using high-resolution 2-dimensional wavenumber and K-line spectra. These spectra were computed at frequencies of 0.067, 0.101, 0.134, 0.168, 0.202, and 0.236 Hz.

K-line spectra were computed for each of the three arms shown in Figure 15. The crosspower matrix for each arm was obtained from an average of the crosspower from sensors in all lines parallel to the arms. The spectra from the three arms were collectively analyzed to determine the spatial organization of the noise.

The first frequency at which a relatively low prediction error was obtained is 0.168 Hz. The spectra show two noise lobes to be the principal contributors to the total noise field. Surface-mode energy from N60°E with a velocity of 3.1 km/sec is the slightly stronger contributor. P-wave energy from the south with an apparent velocity of approximately 40 km/sec is the second principal contributor.

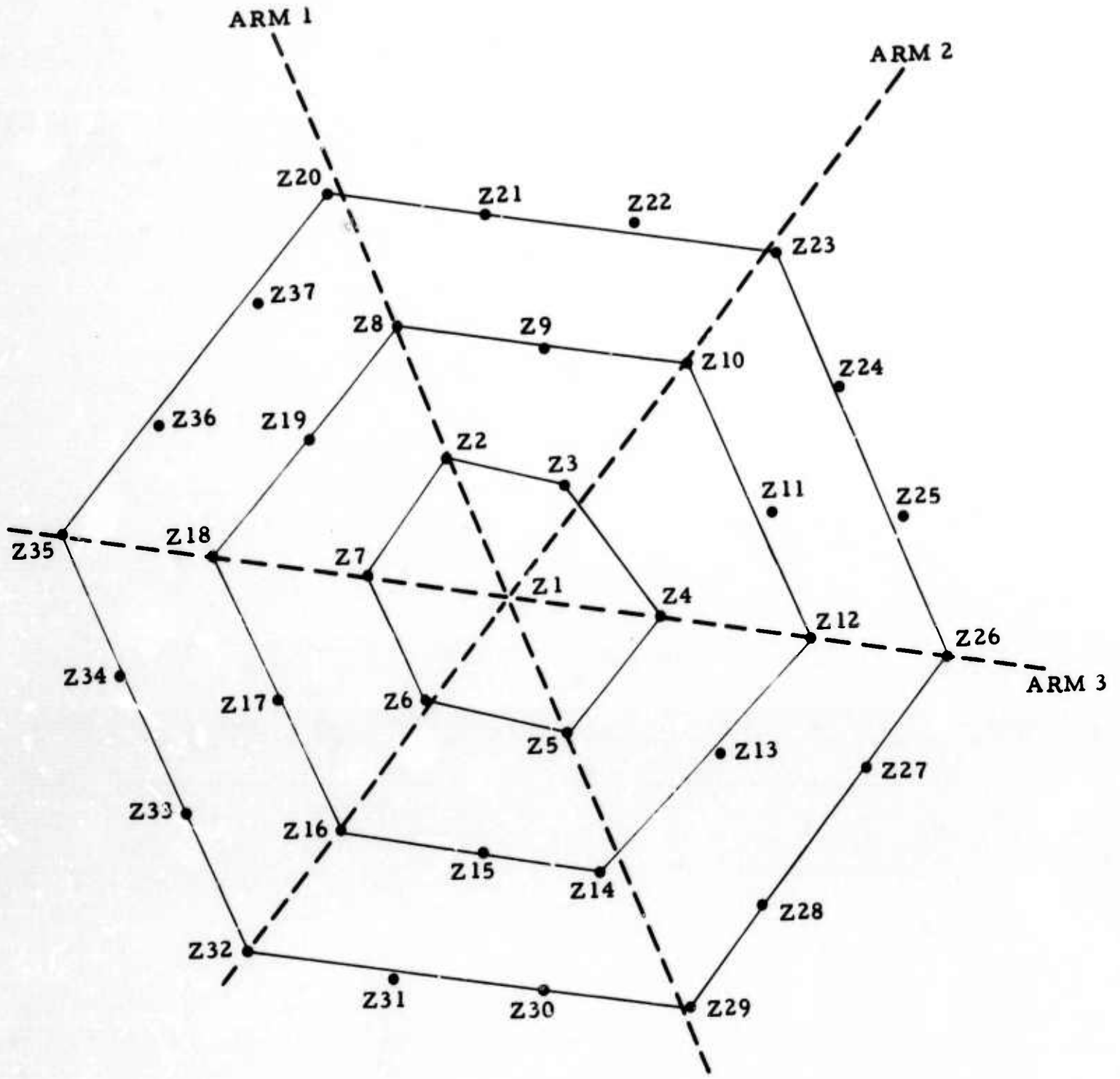

Figure 15. Extended Short-Period Array at TFO

At 0.203 Hz, P-wave energy becomes the strongest contributor to the coherent noise field. The surface-mode energy is still a strong contributor at 0.203 Hz; however, at the next frequency, 0.236 Hz, the surface-mode contribution is very small and P-wave energy from the south becomes dominant at the higher frequencies.

A high-resolution 2-dimensional wavenumber spectrum computed at the frequency of 0.168 Hz is presented in Figure 16. P-wave energy from the south and the surface-mode energy from the northeast is evident. Significant energy from the southwest and possibly southeast is also indicated. Velocities measured from the spectrum agree with those from the K-line spectra.

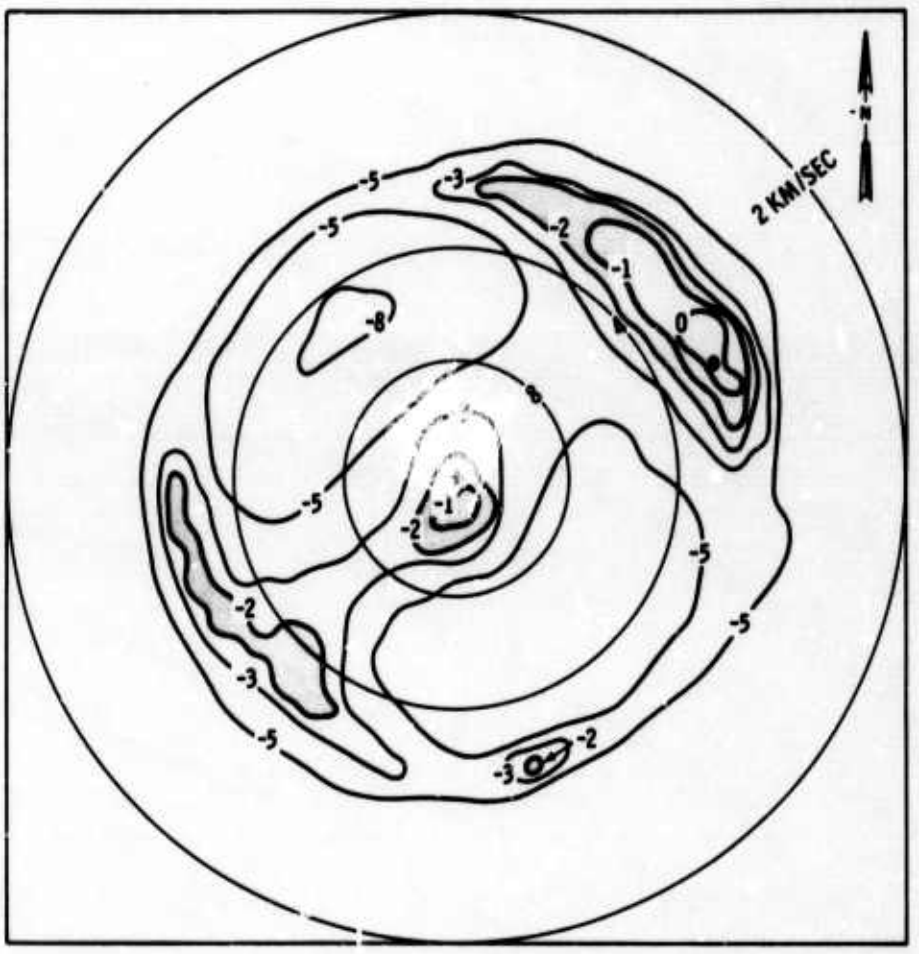

Figure 16. High-Resolution Wavenumber Spectra of "Summer" Noise at 0.168 Hz Frequency

B. WINTER NOISE ANALYSIS

To compare the winter noise to the summer noise, the winter noise analysis is like that of the summer noise. In general, the winter noise appears to have much higher coherent energy at the lower frequencies.

K-line spectra computed at 0.122 Hz frequency show a very low prediction error. Interpretation of the spectra indicate that possibly four or five surface-mode contributors exist in the spectra. The principal contributor is from S20°E with an apparent velocity of 3.13 km/sec. Secondary contributors are from the northwest, southwest, and northeast. At the next frequency, 0.163 Hz, the surface-mode energy from the southwest becomes the primary surface-mode contributor. A high-resolution wavenumber spectrum computed at this frequency is shown in Figure 17. This spectrum also reveals a P-wave contributor from the northwest with significant power. Wavenumber spectra from the next frequency, 0.203 Hz, shows the P-wave energy from the northwest to be the principal contributor. The surface-mode contributor from the northeast is now the primary surface-mode contributor and remains evident in the spectra through the frequency of 0.284 Hz where the P-wave is quite dominant.

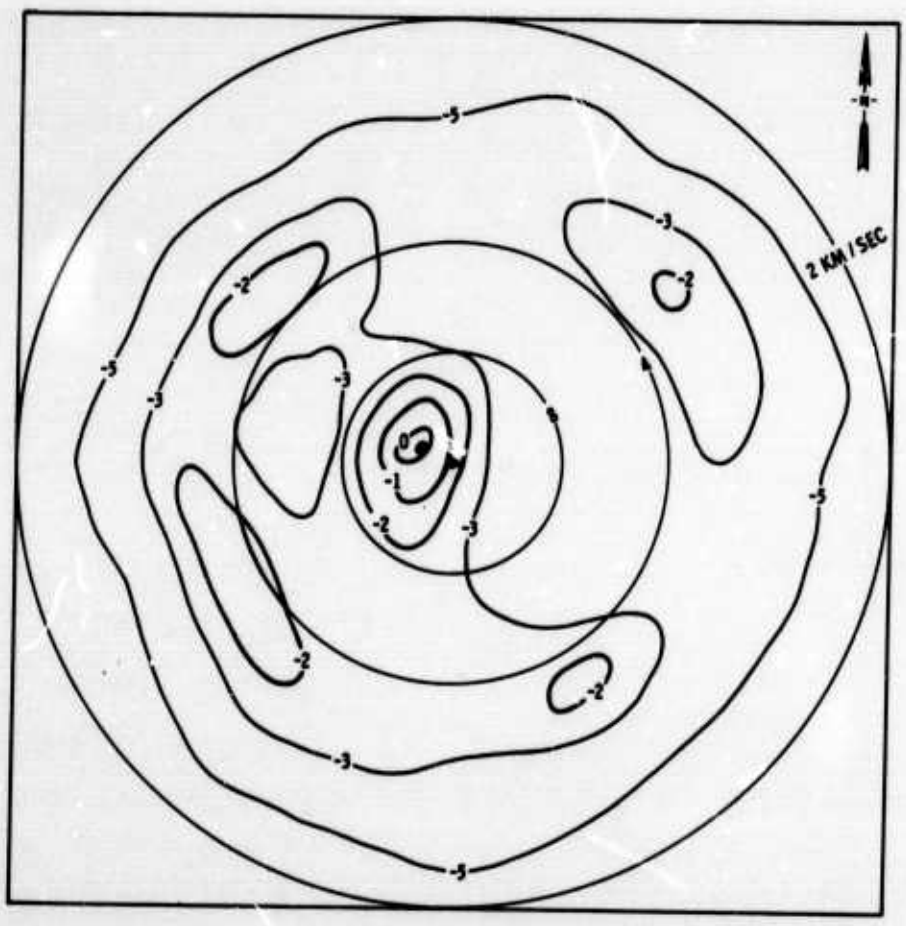

Figure 17. High-Resolution Wavenumber Spectra of "Winter" Noise at 0.163 Hz Frequency

C. MULTICHANNEL PROCESSING

Multichannel processing of the extended short-period array was evaluated on both the summer and winter noise samples. The evaluation included the design and application of optimum Wiener filters for the following set of array elements (see Figure 15):

- Innermost ring of sensors, including the center sensor
- Same as above with the addition of the center ring
- All sensors of the extended array (with the exception of three or four sensors which were not operating properly)

Results of the multichannel filtering were compared to a straight-summation process on the same elements.

The signal-to-noise improvement of a straight-summation process on the summer noise for the three subsets of array elements is shown in Figure 18. A low is observed at 0.23 Hz where the wavenumber analysis indicated dominant P-wave energy. Signal-to-noise improvement reaches the $\sqrt{N}$ level for each of the subsets at approximately 1.0 Hz.

Improvement of multichannel filtering over results for the straight-summation process for the summer data is presented in Figure 19. A maximum improvement of 5.6 db relative to beamsteer processing is obtained at 0.13 Hz using 33 elements of the extended array. Above 0.8 Hz, no significant improvements (less than 2 db) is observed.

Multichannel processing of the winter data gave similar results except for a slight increase in the signal-to-noise improvement at low frequencies due to the increase in surface-mode noise in the winter sample.

D. PLANS

The wavenumber analysis of the noise field will be extended to include higher frequencies (up to 0.5 Hz) to study the structure of the P-wave

energy in greater detail. Upon completion of this study, a special report detailing the processing of the data and results will be prepared. A draft of the report should be available during the latter part of March.

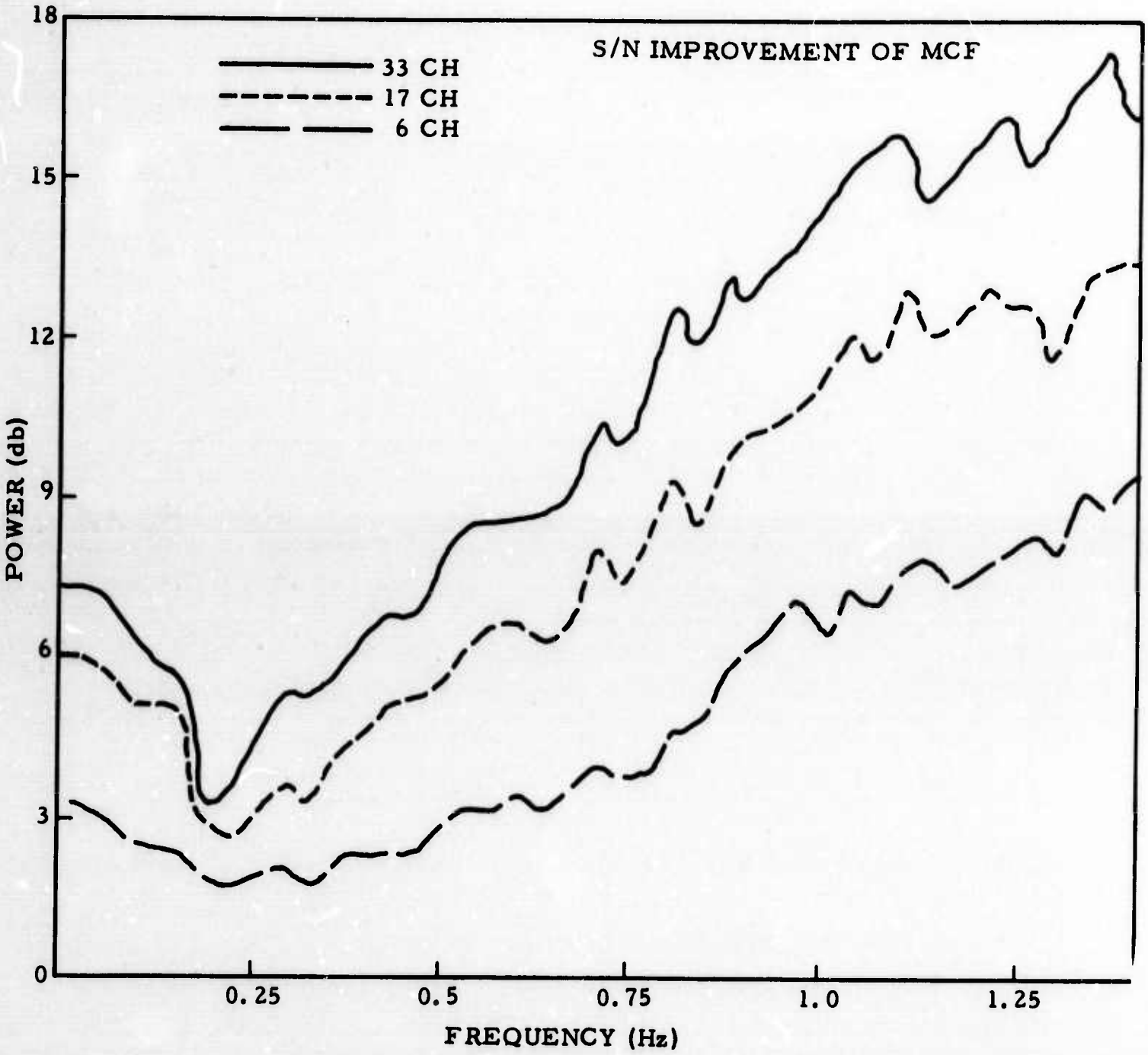

Figure 18. Signal-to-Noise Improvement of Straight-Summation Processing of TFO "Summer" Noise

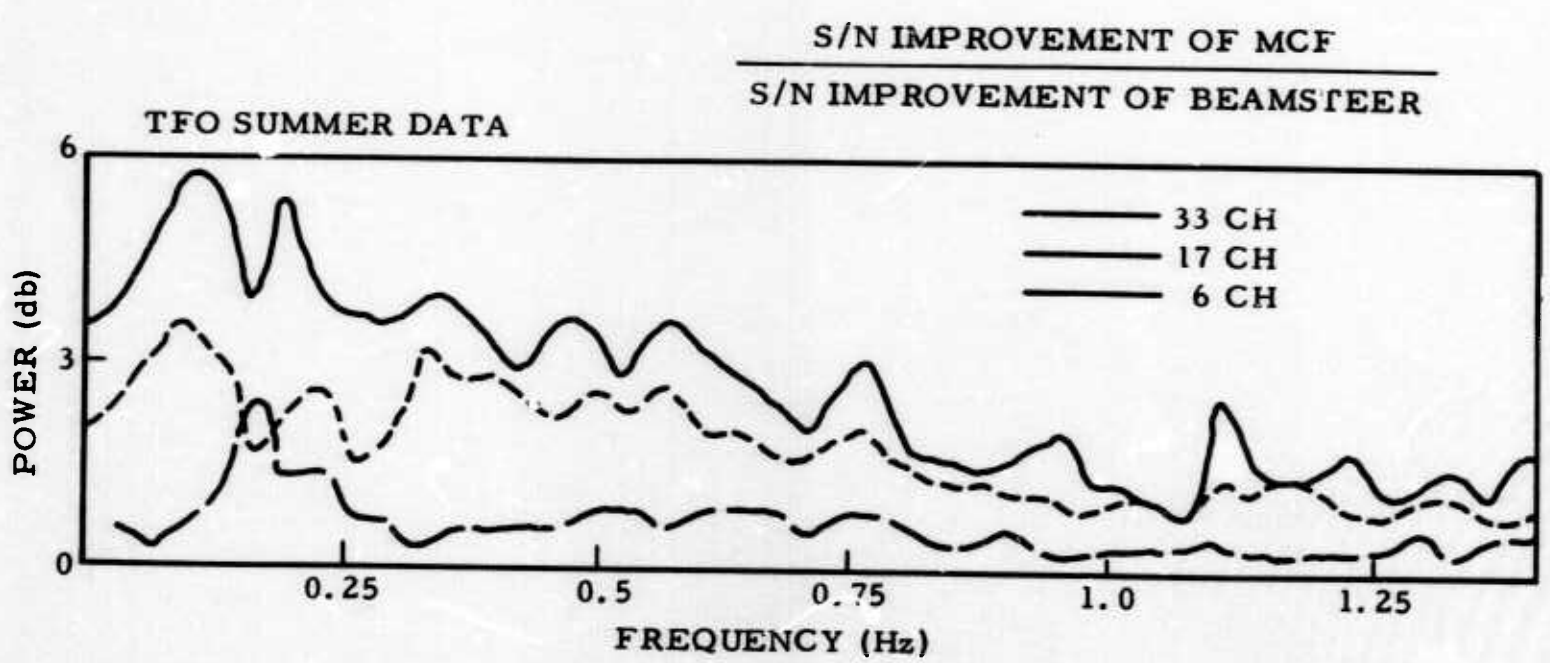

Figure 19. Signal-to-Noise Improvement by Multichannel Filtering over that of Beamsteering on "Summer" Noise

SECTION VI: HIGH-RESOLUTION WAVENUMBER SPECTRA DISPLAY

The objective of this task is to simulate an on-line high resolution wavenumber spectra display.

The equation for the high-resolution spectra is

$$P_H(\vec{V}) = \frac{1}{S^{*T} H^{-1} S}$$

where

S = beamsteer vector for velocity $\vec{V}$

H = crosspower matrix

*T = conjugate transpose

$\vec{V}$ = apparent horizontal velocity

-1 = inverse

For purposes of comparison the conventional beamsteer spectrum will also be computed

$$P_c(\vec{V}) = S^{*T} HS$$

where S, H and V are defined as above.

The original conception of this program was to use the TIAC 870A with a CRT for computation and display. However, because of the relatively small amount of data to be processed and difficulties which have been experienced with the CRT display, it was decided to calculate the spectra on a general purpose machine and use Calcomp plots for display.

The simulation program is designed for use on small (7 km or less) short-period arrays and large (120 km or less) long-period arrays. Two different requirements for the spectra are

- Rapidly changing spectra for signal detection
- Slowly varying spectra for noise analysis

The program will retain certain flexibilities and will not be written to actually simulate the arithmetic operations of an on-line system. Input to the display will be

- Coordinates of the array
- Frequencies at which the spectra will be displayed
- Ability to do a velocity-preserving stack (across frequency) of a wavenumber spectra
- Decay rate of adaptive update of the crosspower matrix
- Addition of spatially random noise to the cross-power matrix

Fixed parameters will be

- Number of channels ≤ 20
- 64-point transforms at a 2.0-sec sampling rate for long-period data
- 64-point transforms at about a 0.1-sec sampling rate for short-period data
- Velocity range of 8 km/sec ≤ V ≤ ∞ for short-period data and 2 km/sec ≤ V ≤ ∞ for long-period data
- A 50-percent gate overlap between successive spectra

The programming for this task has begun and will be completed in March. Adequate short-period and long-period data are available in-house for the simulation.

SECTION VII: SPECIAL PROBLEMS

During the past quarter, two special technical reports have been submitted and approved for printing.

The first, Extraction of Spectral Lines from Seismic Data, discusses two methods for the removal in real-time of stable spectral lines from seismic data. The first method involves the generation of a cosine wave

by means of a digital feedback system to approximate the spectral lines. In this method, the cosine generator is adjusted in accordance with a mean-square-error criterion. This system of adjustment was simulated and proved to be unstable. In the second method, a Widrow adaptive prediction filter is used to remove the deterministic component. A simulation of this prediction method was carried out using one seismic data channel from a short-period array. Results show that this method significantly attenuates some of the spectral lines. However, if a signal were present, some amplitude and phase distortion would be caused in the signal. In addition, this system would be cumbersome to implement.

The second report, Suboptimal Multichannel Digital Filters, discusses a new method of generating time-domain filters to extract a signal from digitized multichannel noise. The new filter generation technique is based on the frequency-domain Wiener filter response and uses the mean-square-error of the whole filter set in the transformation back into the time domain. This new, computationally efficient technique was evaluated against a previously used technique, also based on the frequency-domain Wiener filter response. Two different sets of experimental noise data with power spectra specified at 65 frequencies were used in the filter evaluation, and the signal to be detected was assumed to have the same power spectrum as the noise to prevent frequency filtering. For the first noise sample and 37-point long filters, the previous technique gave 0.8 db more error than the optimum frequency-domain filter and the new filtering technique gave 0.5 db more error. For the second noise sample, these respective filters had 1.2 db and 0.9 db more error than the optimum technique. These reports will be printed during February.

No further work is contemplated under special problems.

UNCLASSIFIED
Security Classification

DOCUMENT CONTROL DATA - R & D

(Security classification of title, body of abstract and indexing annotation must be entered when the overall report is classified)

1. ORIGINATING ACTIVITY *(Corporate author)*
Texas Instruments Incorporated
Science Services Division
P.O. Box 5621, Dallas, Texas 75222

2a. REPORT SECURITY CLASSIFICATION
Unclassified

2b. GROUP
None

3. REPORT TITLE
SEISMIC ARRAY PROCESSING TECHNIQUES, QUARTERLY REPORT NO. 2

4. DESCRIPTIVE NOTES *(Type of report and inclusive dates)*
Quarterly Report No. 2, 15 November 1969 through 15 February 1970

5. AUTHOR(S) *(First name, middle initial, last name)*
Frank H. Binder, Program Manager

6. REPORT DATE	7a. TOTAL NO. OF PAGES	7b. NO. OF REFS
3 March 1970	41	4

8a. CONTRACT OR GRANT NO.	9a. ORIGINATOR'S REPORT NUMBER(S)
F 33657-70-C-0100	
b. PROJECT NO. VELA/T/0701/B/ASD	
c.	9b. OTHER REPORT NO(S) *(Any other numbers that may be assigned this report)*
d.	

10. DISTRIBUTION STATEMENT
This document is subject to special export controls and each transmittal to foreign governments or foreign nationals may be made only with prior approval of Chief, AFTAC.

11. SUPPLEMENTARY NOTES	12. SPONSORING MILITARY ACTIVITY
ARPA Order No. 624	Advanced Research Projects Agency Department of Defense The Pentagon, Washington, D.C. 20301

13. ABSTRACT

This second quarterly report discusses progress and initial results in the categories of adaptive techniques for designing fixed filters off-line, on-line adaptive processing techniques, long-period array data analysis, short-period 37-element array data analysis, Hi Resolution wavenumber spectra displays of seismic array data, and suboptimal multichannel digital filters.

DD FORM 1 NOV 65 1473

UNCLASSIFIED
Security Classification

14. KEY WORDS	LINK A		LINK B		LINK C	
	ROLE	WT	ROLE	WT	ROLE	WT
Seismic array processing techniques						
Adaptive MCFs						
On-line adaptive multichannel processing						
Methods for spectral line removal						
Suboptimal multichannel digital filters						